Atmos. Chem. Phys. Discuss., 14, 22587–22638, 2014
www.atmos-chem-phys-discuss.net/14/22587/2014/
doi:10.5194/acpd-14-22587-2014

Atmospheric Chemistry and Physics Discussions

Constraining terrestrial ecosystem CO_2 fluxes by integrating models of biogeochemistry and atmospheric transport and data of surface carbon fluxes and atmospheric CO_2 concentrations

Q. Zhu[1,2,*], Q. Zhuang[1,2,3], D. Henze[4], K. Bowman[5,6], M. Chen[7], Y. Liu[1,2], Y. He[1,2], H. Matsueda[8], T. Machida[9], Y. Sawa[8], and W. Oechel[10]

[1]Purdue Climate Change Research Center, Purdue University, West Lafayette, Indiana, USA
[2]Department of Earth, Atmospheric, and Planetary Sciences, Purdue University, West Lafayette, Indiana, USA
[3]Department of Agronomy, Purdue University, West Lafayette, Indiana, USA
[4]Department of Mechanical Engineering, University of Colorado, Boulder, Colorado, USA
[5]Jet Propulsion Laboratory, California Institute of Technology, Pasadena, California, USA

[6]Joint Institute for Regional Earth System Science and Engineering, University of California, Los Angeles, California, USA
[7]Department of Organismic & Evolutionary Biology, Harvard University, Cambridge, Massachusetts, USA
[8]Geochemical Research Department, Meteorological Research Institute, Tsukuba, Japan
[9]National Institute for Environmental Studies, Tsukuba, Japan
[10]Biology Department, San Diego State University, San Diego, California, USA
[*]now at: Lawrence Berkeley National Lab, Berkeley, California, USA

Received: 19 June 2014 – Accepted: 15 August 2014 – Published: 3 September 2014

Correspondence to: Q. Zhu (qzhu@lbl.gov)

Published by Copernicus Publications on behalf of the European Geosciences Union.

ACPD
14, 22587–22638, 2014

Abstract

Regional net carbon fluxes of terrestrial ecosystems could be estimated with either biogeochemistry models by assimilating surface carbon flux measurements or atmospheric CO_2 inversions by assimilating observations of atmospheric CO_2 concentrations. Here we combine the ecosystem biogeochemistry modeling and atmospheric CO_2 inverse modeling to investigate the magnitude and spatial distribution of the terrestrial ecosystem CO_2 sources and sinks. First, we constrain a terrestrial ecosystem model (TEM) at site level by assimilating the observed net ecosystem production (NEP) for various plant functional types. We find that the uncertainties of model parameters are reduced up to 90 % and model predictability is greatly improved for all the plant functional types (coefficients of determination are enhanced up to 0.73). We then extrapolate the model to a global scale at a $0.5^\circ \times 0.5^\circ$ resolution to estimate the large-scale terrestrial ecosystem CO_2 fluxes, which serve as prior for atmospheric CO_2 inversion. Second, we constrain the large-scale terrestrial CO_2 fluxes by assimilating the GLOBALVIEW-CO2 and mid-tropospheric CO_2 retrievals from the Atmospheric Infrared Sounder (AIRS) into an atmospheric transport model (GEOS-Chem). The transport inversion estimates that: (1) the annual terrestrial ecosystem carbon sink in 2003 is $-2.47\,\mathrm{Pg\,C\,yr^{-1}}$, which agrees reasonably well with the most recent inter-comparison studies of CO_2 inversions ($-2.82\,\mathrm{Pg\,C\,yr^{-1}}$); (2) North America temperate, Europe and Eurasia temperate regions act as major terrestrial carbon sinks; and (3) The posterior transport model is able to reasonably reproduce the atmospheric CO_2 concentrations, which are validated against Comprehensive Observation Network for TRace gases by AIrLiner (CONTRAIL) CO_2 concentration data. This study indicates that biogeochemistry modeling or atmospheric transport and inverse modeling alone might not be able to well quantify regional terrestrial carbon fluxes. However, combining the two modeling approaches and assimilating data of surface carbon flux as well as atmospheric CO_2 mixing ratios might significantly improve the quantification of terrestrial carbon fluxes.

ACPD
14, 22587–22638, 2014

1 Introduction

Atmospheric carbon dioxide (CO_2) concentrations have greatly increased since the pre-industrial era, which is primarily due to increasing anthropogenic emissions of CO_2 (Marland et al., 2003) and human-induced land-use and land-cover changes (Houghton, 2003; Kaul et al., 2009). Observations reveal that the rapid increase of atmospheric CO_2 modified the energy balance of the earth system through a positive radiative forcing effect and warmed up the climate system (Forster et al., 2007). The warming effect is mitigated through removing the atmospheric CO_2 by oceans (Jacobson et al., 2007a; Sabine et al., 2004) and terrestrial ecosystems (Saeki et al., 2013; Yu et al., 2013). Recent studies estimate that about $8.3 \pm 0.4\,\mathrm{Pg\,C\,yr^{-1}}$ ($1\,\mathrm{Pg} = 10^{15}\,\mathrm{g}$) is released by fossil-fuels burning and cement production (E_{FF}) (Le Quéré et al., 2013) during the recent decade. The oceans take up about $2.5 \pm 0.5\,\mathrm{Pg\,C\,yr^{-1}}$, which accounts for 30 % of the anthropogenic E_{FF} emissions (Takahashi et al., 2009; Wanninkhof et al., 2012); the terrestrial ecosystems absorb about $2.6 \pm 0.8\,\mathrm{Pg\,C\,yr^{-1}}$, which accounts for 31 % of the E_{FF} emissions (Sitch et al., 2013). Although the oceanic reservoir and the terrestrial biosphere absorb a roughly equal amount of anthropogenic emissions of CO_2 on a decadal scale, the oceanic carbon flux is relatively stable in terms of seasonal variability, inter-annual trend and spatial distribution (Le Quéré et al., 2009; Takahashi et al., 2009) and plays a minor role in controlling the temporal and spatial variations of atmospheric CO_2 concentrations. In contrast, the terrestrial ecosystem carbon budgets have a much larger temporal variability and spatial heterogeneity, due to the complex non-linear responses of ecosystem carbon dynamics to the changing climate (Jung et al., 2011; Medvigy et al., 2010; Sitch et al., 2008, 2013). The variations of atmospheric CO_2 concentrations are dominated by the magnitude and distribution of terrestrial ecosystem carbon uptake rather than the oceanic uptake. Therefore, it is fundamentally important to quantitatively understand the current terrestrial ecosystem carbon budgets and their inter-annual trend, seasonal variation and spatial distribution, in order to better project future levels of atmospheric concentrations.

ACPD
14, 22587–22638, 2014

Regional and global terrestrial ecosystem carbon budgets have been extensively studied and revisited over the past three decades mainly through two approaches: (1) process-based ecosystem biogeochemistry modeling (Z. Chen et al., 2013; Melillo et al., 1993; Sitch et al., 2013) and (2) atmospheric CO_2 inverse modeling (Gurney et al., 2002; Kaminski and Heimann, 2001; Peters et al., 2007; Peylin et al., 2013; Tans et al., 1989). The biogeochemistry modeling, so called bottom-up approach, simulates the ecosystem carbon dynamics including photosynthesis, plant respiration and soil respiration (Knorr and Heimann, 2001; Luo et al., 2003; Sierra et al., 2007; Sitch et al., 2008; Zhuang et al., 2003). The net CO_2 budget or net ecosystem production (NEP) (Randerson et al., 2002) is calculated as the difference between photosynthesis and ecosystem respirations (plant respiration plus soil respiration). Atmospheric CO_2 inversion (top-down approach) is another useful tool to investigating large-scale carbon budgets. This approach is based on the observed atmospheric CO_2 concentration data and transport models to infer the magnitude and spatial distribution of surface carbon sources and sinks (Chevallier and O'Dell, 2013; Gurney et al., 2002; Peters et al., 2007). To date, it is still challenging to quantify the regional patterns of terrestrial carbon exchanges using this approach (Janssens et al., 2005; Peylin et al., 2013; Piao et al., 2009; Sierra et al., 2007). Recent atmospheric CO_2 inversion studies show considerably diverse results. For example, northern terrestrial ecosystems are estimated as a carbon sink ranging from 0.5 to 4 Pg C yr^{-1} while tropical terrestrial ecosystems act as a carbon sink of 1 Pg C yr^{-1} or a carbon source up to 4 Pg C yr^{-1} (Gurney et al., 2004; Jacobson et al., 2007b; Peylin et al., 2002, 2013; Rödenbeck et al., 2003; Stephens et al., 2007).

One of the most significant limitations of CO_2 inversion modeling is that there is no sufficient CO_2 concentration data (Dargaville et al., 2006). For example, in the Atmospheric Tracer Transport Model Intercomparison Project 3 (TransCom 3) (Gurney et al., 2008), large areas over lands and tropics were not well observed by its CO_2 network. Thus, the uncertainties of estimated carbon fluxes were generally larger in these areas than over the oceans (Gurney et al., 2002). One possible solution is to use alterna-

ACPD
14, 22587–22638, 2014

tive satellite-based CO_2 observations, which have much larger spatial coverage (Basu et al., 2013; Deng et al., 2014; Houweling et al., 2004; Nassar et al., 2011). Although satellite-based CO_2 retrievals were less precise than in situ CO_2 measurements, previous studies have demonstrated that their large spatial coverage could benefit the surface flux estimations (Basu et al., 2013; Chevallier and O'Dell, 2013; Houweling et al., 2004; Nassar et al., 2011).

Atmospheric CO_2 inversions are also highly sensitive to land surface prior fluxes (Dargaville et al., 2006; Peylin et al., 2013). Realistic prior terrestrial ecosystem flux data (magnitude and uncertainty) are critical to resolving the ill-posed problem of CO_2 inversions (Kaminski and Heimann, 2001), ensure that the posterior estimations are biogeochemically reasonable, and impose a strong constraint over the regions where observations are sparse or highly uncertain (Gurney et al., 2008). Biogeochemistry models have proven to be useful tools to generate the prior carbon flux for the CO_2 inversion studies. For example, Nassar et al. (2011) used re-gridded 1° by 1° resolution annual balanced NEP (annual flux 0 Pg C) simulated by Carenegie Ames Stanford Approach (CASA) and an annual terrestrial exchange climatology (annual flux −5.29 Pg C). However, such prior carbon flux does not consider year-to-year variation. In reality, the terrestrial ecosystem carbon dynamics are highly sensitive to the environmental conditions of temperature, precipitation and radiation. The interannual variability of terrestrial ecosystem carbon flux could be as large as their annual mean (Dargaville et al., 2006). FLUXNET network (Baldocchi, 2008; Baldocchi et al., 2001) observed carbon flux has also been widely used to improve the estimations of prior flux for CO_2 inversions (Chevallier et al., 2012; Knorr and Kattge, 2005). Although FLUXNET in situ observations only provide knowledge within a footprint up to a few kilometers (Baldocchi, 2003; Schmid, 1994), the local information could be scaled up to regions using biogeochemistry models. All in all, combining FLUXNET in situ observations as well as biogeochemistry model is an effective way to generate reliable prior carbon flux for the CO_2 inversion.

ACPD
14, 22587–22638, 2014

In this study, we aim to quantify terrestrial ecosystem carbon budget at sub-continental scales with a two-phase framework by combining TEM bottom-up biogeochemistry modeling (Zhu and Zhuang, 2013a) and GEOS-Chem top-down CO_2 inversion (Henze et al., 2007). Our first objective focuses on obtaining reliable terrestrial ecosystem carbon flux estimates, which will serve as a prior for the GEOS-Chem inversion, by assimilating the AmeriFlux data into a biogeochemistry model TEM. Our second objective attempts to assimilate the GLOBALVIEW-CO2 surface CO_2 concentrations (Globalview-CO2, 2013) and mid-troposphere CO_2 concentrations retrieved from Atmospheric Infrared Sounder (AIRS) (Chahine et al., 2008; Chevallier et al., 2009; Maddy et al., 2008; Tiwari et al., 2006) into GEOS-Chem to further constrain the regional terrestrial ecosystem carbon budgets.

2 Methodology

2.1 Overview

In this study, we combine process-based biogeochemistry modeling (bottom-up approach) and atmospheric CO_2 inverse modeling (top-down approach) to quantify the terrestrial ecosystem carbon budgets (Fig. 1). We estimate the carbon flux with a two-phase framework, into which multiple sources of observational data are assimilated. In phase one, we assimilate the AmeriFlux network observed NEP data into the terrestrial ecosystem model (TEM) (Zhuang et al., 2010, 2003) to constrain the model parameters for eight representative plant functional types (PFTs) with the adjoint method (Zhu and Zhuang, 2013b, 2014). The constrained model is employed to simulate the global terrestrial ecosystem carbon budgets at a 0.5° by 0.5° resolution. The carbon flux is integrated to 4° by 5° (latitude by longitude) resolution and serves as the prior constraint for the transport inversion. In phase two, the GLOBALVIEW-CO2 (Globalview-CO2, 2013) surface CO_2 concentrations and AIRS mid-troposphere CO_2 retrievals (Chahine et al., 2008; Maddy et al., 2008) are assimilated into an atmospheric transport model

ACPD
14, 22587–22638, 2014

(GEOS-Chem) (Nassar et al., 2010) with its adjoint version (Henze et al., 2007) to further constrain our prior estimations of terrestrial CO_2 fluxes. The posterior terrestrial ecosystem CO_2 budgets constrained by AmeriFlux NEP data and GLOBALVIEW-CO2 and AIRS CO_2 data are finally evaluated at 11 land regions defined by the TransCom 3 standard (Gurney et al., 2008). The posterior CO_2 concentrations are evaluated at several representative inland GLOBALVIEW-CO2 sites as well as CONTRAIL airplane samplings locations between Japan and Australia.

2.2 Adjoint-TEM and AmeriFlux NEP

The Terrestrial Ecosystem Model (TEM) is a biogeochemistry model that simulates the ecosystem carbon and nitrogen fluxes and pools (McGuire et al., 1992; Zhuang et al., 2010, 2003) (Please see Appendix A for more details of TEM). The Adjoint-TEM is a data assimilation version of TEM based on the adjoint method (Giering and Kaminski, 1998). It is able to assimilate in situ AmeriFlux NEP data (Zhu and Zhuang, 2014) and the MODIS remote sensing GPP product (Zhu and Zhuang, 2013a). Observational data are fused into TEM through minimizing a pre-defined cost function (J), which comprises a prior part (J_{prior}) and an observational part (J_{obs}).

$$J = J_{\text{prior}} + J_{\text{obs}} \tag{1}$$

$$J_{\text{prior}} = (\boldsymbol{p} - \boldsymbol{p}^{\mathbf{o}})^T \boldsymbol{S}^{-1} (\boldsymbol{p} - \boldsymbol{p}^{\mathbf{o}}) \tag{2}$$

$$J_{\text{obs}} = \sum_{i=1}^{N} (f(x)_i - f_i^{\text{o}})^T R_i^{-1} (f(x)_i - f_i^{\text{o}}) \tag{3}$$

where $\boldsymbol{p}$ and $\boldsymbol{p}^{\mathbf{o}}$ are vectors of the updated and prior parameters, respectively. Fifteen model parameters associated with the processes of interest (Table 1) are constrained in this study. $\boldsymbol{S}^{-1}$ is the inverse of prior parameter uncertainty. We assume: (1) there are no correlations between parameters (off-diagonal elements of $\boldsymbol{S}$ are zeros); (2) variances of prior parameters (diagonal elements of $\boldsymbol{S}$) are 40 % of the difference be-

ACPD
14, 22587–22638, 2014

tween their upper and lower bounds (Kuppel et al., 2012). $f(x)_i$ and f_i^o are simulated and observed NEP, respectively, at time step i. $i \in [1, N]$ covers the assimilation time window and N is the total amount of NEP data that have been assimilated. R_i^{-1} is the inverse of AmeriFlux NEP observational error, which is assumed to be 20 % of the observed NEP (Raupach et al., 2005).

The cost function penalizes misfit between modeled and observed NEP (Eq. 3) and ensures the updated model parameters are biogeochemically reasonable according to our prior knowledge (Eq. 2). The adjoint-TEM data assimilation is a gradient-based optimization approach. The role of the adjoint version of TEM is to calculate the first order derivative of the cost function with respect to model parameters ($\frac{\partial \boldsymbol{J}}{\partial \boldsymbol{p}}$). A quasi-Newton method Broyden–Fletcher–Goldfarb–Shanno (BFGS) (Broyden, 1970) is employed to minimize the cost function and optimize model parameters. The posterior parameter uncertainty is calculated using Eq. (4) with linearity approximation at the minimum of the cost function (Kaminski et al., 2002; Kuppel et al., 2012).

$$\boldsymbol{R}^{\mathbf{post}} = \left(\sum_{i=1}^{N} \boldsymbol{H}_{\mathbf{i}}^T R_i^{-1} \boldsymbol{H}_{\mathbf{i}} + \boldsymbol{S}^{-1} \right)^{-1} \tag{4}$$

where i starts from 1 to N, covering the entire assimilation time window. R_i and $\boldsymbol{S}$ are observation error and parameter prior error covariance matrix, respectively. $\boldsymbol{H}_{\mathbf{i}}$ is the Jacobian matrix at the minimum of the cost function J.

The AmeriFlux network samples high-frequency atmospheric turbulence that transports CO_2 across the canopy–atmosphere interface. The net CO_2 exchange is determined by the covariance between the fluctuation of vertical wind velocity and the change of CO_2 mixing ratio using eddy covariance technique (Baldocchi, 2003). The scale (footprint) of AmeriFlux NEP ranges from a few hundred meters to several kilometers (Schmid, 1994), depending on the instrument height, the steadiness of environmental conditions and the flatness of the terrain. The temporal resolution of AmeriFlux NEP data varies from hourly to monthly. We use Level-4 monthly gap-filled NEP

ACPD
14, 22587–22638, 2014

product. The adjoint-TEM data assimilation framework is applied to eight AmeriFlux sites (Table 2) for different representative plant functional types (PFTs). These include tundra, boreal forest, temperate coniferous forest, temperate deciduous forest, grass, shrub, tropical forest, and xeric woodland.

For each PFT, the optimized model is extrapolated to another AmeriFlux site (not used in the assimilation) with the same PFT to evaluate the constrained model. After the cross-site validation, we extrapolate the calibrated TEM to simulate the regional carbon budget. The associated uncertainty of the regional carbon flux is estimated with ensemble model simulations: (1) We sample parameters from the posterior distributions of model parameters (assume to follow the Gaussian distribution with mean of optimal parameter value and variance of posterior uncertainty), which are estimated by the adjoint-TEM framework; (2) For each ensemble, we run forward TEM simulation and obtain a NEP map at 0.5° by 0.5° resolution; (3) We integrate the NEP results to 4° by 5° (latitude by longitude) resolution grids, which is consistent with our GEOS-Chem simulations; and (4) By analyzing the results of TEM modeled NEP at 4° by 5° resolution, we calculate the statistical mean (μ) and variance σ^2 and use them as prior constraints in the GEOS-Chem CO_2 inversion.

2.3 GEOS-Chem CO_2 inversion

GEOS-Chem is a global 3-D atmospheric transport and chemistry model (Bey et al., 2001) that is driven by assimilated meteorological data from the Goddard Earth Observing System (GEOS) of the NASA Global Modeling Assimilation Office (GMAO). The GEOS-Chem CO_2 simulation was first developed by Suntharalingam et al. (2004) and further improved by Nassar et al. (2010) in terms of CO_2 emissions inventories and chemical production of CO_2 sources. GEOS-Chem simulates the time-space evolution of atmospheric CO_2 mixing ratios driven by surface CO_2 fluxes of fossil fuel and cement manufacture emissions (Andres et al., 2011), biomass burning emission (van der Werf et al., 2006), bio-fuel burning emission (Yevich and Logan, 2003), shipping and aviation emissions (Corbett and Koehler, 2003; Friedl, 1997), chemical sources from

ACPD
14, 22587–22638, 2014

oxidation of other carbon species (e.g., CO, CH_4) (Nassar et al., 2010), ocean CO_2 fluxes (Takahashi et al., 2009) and terrestrial ecosystem CO_2 flux (TEM modeled NEP in this study). We use GEOS-4 driving dataset (Bloom et al., 2005) to run GEOS-Chem at a horizontal resolution of 4° by 5° with a vertical resolution of 30 layers.

The adjoint of GEOS-Chem was originally developed by Henze et al. (2007) focusing on aerosol chemistry and thermodynamics. It was further updated and applied to conduct sensitivity analyses of ozone (O_3) (Singh et al., 2011; Zhang et al., 2009), assimilate atmospheric trace gases such as carbon monoxide (CO) (Kopacz et al., 2006) and methane (CH_4) (Wecht et al., 2012). Here, we apply GEOS-Chem adjoint (version v34) to assimilate atmospheric CO_2 concentration data and inverse terrestrial ecosystem carbon fluxes. The adjoint GEOS-Chem data assimilation is a four dimensional variational (4-D-Var) framework that assimilates the whole CO_2 dataset (over space and time) at once. A cost function that describes the time-space discrepancy between GEOS-Chem model simulated and observed CO_2 concentrations is defined as:

$$J(x) = (\boldsymbol{x} - \boldsymbol{x^0})^T \boldsymbol{S}^{-1} (\boldsymbol{x} - \boldsymbol{x^0}) + \sum_{i=1}^{M} \sum_{j=1}^{N} (f(x)_{i,j} - f^0_{i,j})^T R^{-1}_{i,j} (f(x)_{i,j} - f^0_{i,j}) \quad (5)$$

where $\boldsymbol{x}$ and $\boldsymbol{x^o}$ are updated and prior control variables. Since we are interested in only the terrestrial ecosystem component of global CO_2 budgets, $\boldsymbol{x}$ denotes the updated terrestrial ecosystem carbon flux and $\boldsymbol{x^0}$ is our prior estimation of NEP from TEM (μ, estimated in Sect. 2.2). $\boldsymbol{S}^{-1}$ represents the uncertainty of our prior $\boldsymbol{x^0}$. To simplify the inverse modeling, we neglect the correlations between NEP at different locations. Therefore, the off-diagonal elements of $\boldsymbol{S}$ are zeros and the diagonal elements are derived from TEM ensemble simulations (σ^2, estimated in Sect. 2.2). $f(x)_{i,j}$ is an observation operator applied to ecosystem carbon flux $\boldsymbol{x}$, which results in a comparable quantity with the observations at time i space j ($f^0_{i,j}$: in this case are the GLOBALVIEW-CO2 and AIRS CO_2). Only a subset of the GLOBALVIEW-CO2 network (Fig. 2) is selected for the surface flux inversion. Six representative inland sites are reserved for validation

ACPD
14, 22587–22638, 2014

purpose (Table 3). $R_{i,j}^{-1}$ is the inverse of the data error, which is provided by the AIRS CO_2 and GLOBALVIEW-CO2 datasets.

The GEOS-Chem CO_2 inverse modeling is a numerical problem of minimizing $J(x)(x = \mathrm{argmin}(J(x)))$. The optimization is implemented by the L-BFGS-B optimization routine (Byrd et al., 1995), which is a limited memory and bound constraint variant of classic BFGS method (Broyden, 1970). The GEOS-Chem adjoint efficiently calculates the gradient of the cost function with respect to terrestrial ecosystem carbon flux ($\nabla_{\boldsymbol{x}}\boldsymbol{J}$):

$$\nabla_{\boldsymbol{x}}\boldsymbol{J} = \boldsymbol{S}^{-1}(\boldsymbol{x} - \boldsymbol{x^0}) + \sum_{i=1}^{M}\sum_{j=1}^{N} \nabla_{\boldsymbol{x}}\boldsymbol{f}(x_{i,j})^T R_{i,j}^{-1}(f(x_{i,j}) - f^0) \tag{6}$$

where $\nabla_{\boldsymbol{x}}\boldsymbol{f}(x_{i,j})$ represents the gradient of observation operator at time space location (i, j) with respect to surface ecosystem carbon fluxes. For more detailed information about calculating $\nabla_{\boldsymbol{x}}\boldsymbol{J}$ and the construction of the adjoint model, please refer to Henze et al. (2007).

The posterior error covariance matrix is estimated with the inverse of the Hessian (the second derivative of cost function with respect to surface ecosystem carbon fluxes):

$$\boldsymbol{R}^{\mathbf{post}} = \left(\boldsymbol{S}^{-1} + \sum_{i=1}^{M}\sum_{j=1}^{N} \nabla_{\boldsymbol{x}}\boldsymbol{f}(x_{i,j})^T R_{i,j}^{-1} \nabla_{\boldsymbol{x}}\boldsymbol{f}(x_{i,j})\right)^{-1} \tag{7}$$

The inverse of the Hessian is approximated by employing the Davidon–Fletcher–Powell (DFP) algorithm, which had been implemented in GEOS-Chem inverse modeling framework (Deng et al., 2014).

In order to compare our results with previous work, the posterior terrestrial ecosystem carbon fluxes are aggregated and evaluated at 11 sub-continental regions based

ACPD
14, 22587–22638, 2014

on the TransCom 3 standard. We conduct two CO_2 inversions: (1) using CASA balanced biosphere carbon flux and an annual terrestrial exchange climatology (Nassar et al., 2010) as prior; (2) using TEM simulated NEP after assimilating the AmeriFlux observations as prior. Since CASA prior NEP does not provide uncertainties, thus we use the default choice of GEOS-Chem inverse modeling setup and assume the uncertainties to be 50 %. The two inversions are evaluated against several GLOBALVIEW-CO2 sites that were not assimilated and CONTRIAL aircraft CO_2 observations.

2.4 CO_2 concentration data

GLOBALVIEW-CO2 is a data product of the Cooperative Atmospheric Data Integration Project. It is derived from a large number of atmospheric CO_2 concentration measurements with an attempt to resolve the temporal discontinuity and data sparseness (Fig. 2). It compiles CO_2 measurements from different institutions and selects qualified observations based on various baseline conditions (Brunke et al., 2004). The GLOBALVIEW-CO2 product is smoothed, interpolated and extrapolated with a gap-fill technique (Masarie and Tans, 1995). As a result, the CO_2 records in this data product are evenly incremented in time (8 day interval), which greatly facilitates carbon cycle research (D. Baker et al., 2006; Gloor et al., 2000).

In additional to the GLOBALVIEW-CO2 surface network, we also assimilate AIRS mid-troposphere CO_2 retrievals. The Atmospheric Infrared Sounder (AIRS) is an instrument onboard the Aqua satellite, which was launched in 2002 by NASA and is a part of the A-train (afternoon train) satellite constellation. AIRS is operating in a nadir view mode observing the up-welling radiance with a footprint of 13.5 km diameter on the earth surface. The instrument is in a sun-synchronous near-polar orbit with local equatorial crossing time at 1.30 a.m. and 1.30 p.m. (Aumann et al., 2003). The AIRS 2378 hyper-spectral infrared channels ranging from 3.7 µm to 15.4 µm have been widely used to retrieve atmospheric concentrations of ozone, methane, carbon monoxide and carbon dioxide (Chahine et al., 2005; Chevallier et al., 2009; McMillan et al., 2005; Monahan et al., 2007; Xiong et al., 2009) in the mid-to-upper troposphere.

ACPD
14, 22587–22638, 2014

AIRS's ability to retrieve CO_2 is based on the principle that radiances observed in infrared bands (3.7 to 15.4 μm) are sensitive to both temperature and CO_2 concentrations (Chédin et al., 2003). The difficulty is to separate the effects of atmospheric CO_2 concentrations from temperature on the observed radiances. Ideally, if the temperature could be accurately estimated, then the difference between radiative transfer model predicted and AIRS observed radiances could be safely allocated to change of CO_2 concentrations. However, temperature and CO_2 retrievals are interdependent; the error in CO_2 background values could affect temperature retrieval, which in return also affects the CO_2 estimations. This problem is tackled by a minimization procedure that optimizes a prior prescribed CO_2 profile to match the modeled and observed radiances (Tiwari et al., 2006). The AIRS CO_2 retrievals have been extensively evaluated and compared with in situ observations such as NOAA ESRL/GMD aircraft measurements (Maddy et al., 2008), INTEX-NA campaign measurements (Chahine et al., 2008). The comparisons demonstrated that the accuracy of AIRS CO_2 is better than 2 parts per million (ppm).

The AIRS data used in this study is the mid-troposphere CO_2 Level 2 dataset version 5 (Susskind et al., 2011). It is a daily product covering the region mainly from 60° S to 90° N with peak sensitive at from 285 (tropic) to 425 hPa (polar). AIRS averaging kernels are calculated by sequentially perturbing the retrieval at each vertical AIRS defined layers (Olsen, 2009) to assist data assimilation studies. It measures how sensitive a CO_2 retrieval is to changes of CO_2 concentrations at different height. Applying AIRS averaging kernels to GEOS-Chem modeled atmospheric CO_2 ($\boldsymbol{y}_\mathbf{m}$), we will obtain CO_2 concentrations at AIRS retrieval grid ($\hat{\boldsymbol{y}}_\mathbf{m}$).

$$\hat{\boldsymbol{y}}_\mathbf{m} = \boldsymbol{y}_\mathbf{a} + \boldsymbol{A}(\boldsymbol{y}_\mathbf{m} - \boldsymbol{y}_\mathbf{a}) \tag{8}$$

where $\boldsymbol{y}_\mathbf{a}$ and $\boldsymbol{A}$ are AIRS priori and averaging kernel function, respectively.

Besides the six selected GLOBALVIEW-CO2 inland sites that are reserved for validation purpose (Table 3), we also evaluate our posterior CO_2 concentrations with Comprehensive Observation Network for TRace gases by AIrLiner (CONTRAIL) CO_2 datasets

ACPD
14, 22587–22638, 2014

(Machida et al., 2011; Matsueda et al., 2008). The data used in this study are collected by Automatic Air Sampling Equipment (ASE), a flask sampling system installed on Japanese commercial airlines. High precision CO_2 concentrations are sampled at about 10 km altitude over the Pacific Ocean from Japan to Australia. The CONTRAIL CO_2 data in 2003 ranging from 7 January to 18 November contains 22 flights with 12 data points each flight that sampled at different locations. To conveniently compare with GEOS-Chem model outputs, the dataset is grouped into three latitude bins (30° N–10° N, 10° N–10° S, 10° S–30° S).

3 Results and discussion

3.1 Biogeochemical modeling of surface carbon flux

We first present the optimized (posterior) model parameters in terms of statistical mean and uncertainty. Then we compare the posterior parameters against our prior knowledge to investigate how much information we learn through assimilating the AmeriFlux NEP data. The prior-posterior parameters inter-comparisons are conducted at eight AmeriFlux sites with different plant functional types, including tundra, boreal forest, temperate coniferous forest, temperate deciduous forest, grassland, shrubland, tropical forest and xeric woodland. Next, we apply the posterior model to another eight AmeriFlux sites (Table 2), which have the same plant functional type with the parameterization sites, to confirm the effectiveness of model calibration. Then, the posterior model is extrapolated to simulate the global terrestrial ecosystem carbon budgets at a 0.5 ° by 0.5° resolution. Finally, we aggregate the modeled ecosystem carbon budgets according to: (1) eleven land regions defined by the TransCom 3 project and (2) basic plant functional types, in order to conveniently analyze and compare our estimations with previous work.

ACPD
14, 22587–22638, 2014

3.1.1 Model constrained with eddy covariance data

The AmeriFlux NEP measures the net carbon exchange over the canopy–atmosphere interface. It contains information of multiple ecosystem carbon processes: (1) carbon input of photosynthesis; (2) carbon outputs of plant and soil respirations. The nitrogen cycle interacts closely with carbon dynamics in the terrestrial ecosystems. Therefore, the observed net carbon flux also provides constraints on ecosystem nitrogen dynamics to some extent. Model parameters involved in this study are associated with different carbon or nitrogen processes (Table 1). Figure 3 depicts the prior model (grey box) and posterior model (red error bar) in terms of mean and uncertainty (standard deviation). The prior uncertainty is assumed to be 40 % (Kuppel et al., 2012) of the parameter empirical range and the posterior uncertainty is calculated with a linear approximation at the minimum of the cost function.

In general, the AmeriFlux NEP provides more constraint in carbon processes than nitrogen processes (Fig. 3). A majority of nitrogen related parameters have large posterior uncertainties, regardless of the type of plant function. For example, although N_{FALL} (the mean of posterior proportion of vegetation nitrogen loss as litter) differs from its prior mean in some cases, its posterior uncertainty is mostly as high as its prior uncertainty. Within carbon processes, there is no strong evidence showing which particular carbon process (photosynthesis, plant respiration or soil respiration) gained more constraints from the AmeriFlux NEP data (Fig. 3). The extent of posterior model improvement in different carbon processes highly depended on which plant functional type we are dealing with. It further confirms that the AmeriFlux net CO_2 flux is not especially favorable for any particular carbon process. Previous studies have showed that, in principle, net CO_2 flux measurements are difficult to be used to distinguish information from plant or soil respiration or photosynthesis (Knorr and Kattge, 2005; Williams et al., 2009).

Specifically, at tundra and boreal forest sites (two boreal ecosystems), the carbon processes are constrained well, while nitrogen process related parameters are not im-

ACPD
14, 22587–22638, 2014

proved at all. It implies that the model requires additional nitrogen data to constrain the nitrogen dynamics. Another possible reason is that the model structure is potentially deficient in representing the nitrogen cycle of boreal and alpine ecosystems (Zhu and Zhuang, 2013c). Therefore, poorly constrained nitrogen dynamics may not necessarily be attributed to the lack of data. At temperate coniferous and deciduous sites (two temperate forest ecosystems), deciduous forest is relatively better constrained than coniferous forest in terms of carbon processes, especially, for the three photosynthesis parameters maximum photosynthesis rate (C_{MAX}), half saturation constant for PAR (K_I) and half saturation constant for CO_2 (K_C). The nitrogen parameters values are improved to some extent. For example, the posterior mean of maximum rate of *N* uptake (N_{MAX}) is enhanced compared with its prior. However, the posterior uncertainties of the nitrogen parameters are not reduced much at both of the two temperate forest sites. At grass and shrub sites, the photosynthesis parameters of grass ecosystems are better constrained while the soil respiration and nitrogen processes are relatively less improved compared with shrub. The plant respiration parameters are both well constrained at the two sites. At tropical forest, it is interesting to find that the nitrogen processes are well improved except the N_{FALL}. In contrary, at xeric woodland site the nitrogen processes are not improved at all. However carbon processes at this site are generally well improved, except a carbon related litterfall parameter (C_{FALL}) and soil respiration Q10 module parameter (R_{HQ10}). That is because at woodland site (Freeman Ranch Mesquite Juniper) the ecosystem processes are strongly limited by the environmental condition of precipitation (Litvak et al., 2010). Therefore, the observed carbon flux reflects the mechanistic response of carbon dynamics to the water cycle, rather than nitrogen cycle (Heinsch et al., 2004). We speculate that, by using independent nitrogen process associated data; the model could be further improved.

The posterior model is evaluated at independent AmeriFlux sites (Table 2) for each basic plant functional type. Figure 4 depicts the model-data comparison (4a for prior model; 4b for posterior model). We use the coefficient of determination (COD) to com-

ACPD
14, 22587–22638, 2014

pare the prior and posterior model performances against the AmeriFlux observations.

$$\mathrm{COD} = 1 - \frac{\sum_i (y_i - f_i)^2}{\sum_i (y_i - \overline{y})^2} \quad (9)$$

where y_i is the AmeriFlux NEP time series, f_i is model simulated NEP and $\overline{y}$ is averaged NEP observations. COD (or named model efficiency) provides a criterion to quantitatively measure how well a model could replicate the observed time series (Medlyn et al., 2005). In general, COD approaching 1.0 indicates a better model.

The posterior model COD (Fig. 4b) is larger and closer to 1.0 compared with the prior COD (Fig. 4a), regardless of the types of plant function. It indicates that the model predictability is improved by assimilating the AmeriFlux NEP data. Therefore, we conclude that the adjoint based data assimilation framework was effective to improve model performance for various ecosystem types. Large prior-posterior COD differences are observed at forest sites, including boreal forest (COD improved from 0.21 to 0.89), temperate deciduous forest (0.00 to 0.54) and temperate coniferous forest (0.00 to 0.73). The smallest COD improvement is at Lost Creek shrub site (COD only enhanced from 0.26 to 0.33).

3.1.2 Global terrestrial ecosystem carbon budget

The posterior model is scaled up to simulate the global terrestrial ecosystem carbon budget (0.5° by 0.5°) and aggregated to eleven land regions according to the TransCom 3 standard (Gurney et al., 2008). Figure 5 shows the net ecosystem carbon of the eleven sub-continental regions in terms of mean and uncertainty. In 2003, the global terrestrial ecosystem is estimated as a carbon sink of -1.97 ± 1.0 Pg C (negative value means sink). Estimation around 2 Pg C yr^{-1} seems to be robust indicated by previous studies (Houghton, 2007; Le Quéréet al., 2009; Sarmiento et al., 2010; Schimel et al., 2001). For example, Houghton (2007) estimates the terrestrial car-

ACPD
14, 22587–22638, 2014

bon sink to be $-1.9 \pm 1.1\,\mathrm{Pg\,C\,yr^{-1}}$ in the 1980s, $-2.6 \pm 1.1\,\mathrm{Pg\,C\,yr^{-1}}$ in the 1990s and $-2.3 \pm 1.1\,\mathrm{Pg\,C\,yr^{-1}}$ during 2000–2005. The largest terrestrial carbon sink is in North American temperate region ($-0.82 \pm 0.32\,\mathrm{Pg\,C}$). Previous work in 2003 estimates this region as $-0.45 \pm 0.26\,\mathrm{Pg\,C\,yr^{-1}}$ carbon sink (Pacala et al., 2007), which is lower than our estimation. North American boreal region is also a carbon sink of $-0.119 \pm 0.36\,\mathrm{Pg\,C\,yr^{-1}}$, which is close to $-0.08\,\mathrm{Pg\,C\,yr^{-1}}$ carbon sink in Canada in 2003 estimated by Pacala et al. (2007). However, they do not include the carbon budget in Alaska. Taking account of a possible carbon sink around $-0.02\,\mathrm{Pg\,C\,yr^{-1}}$ in Alaska (He et al., 2013), our estimation in North American boreal region is generally consistent with previous estimations. Adding the North America temperate and boreal carbon budgets together, the North American continent accounts for 50 % of the global terrestrial carbon sink.

The second largest carbon sink is in Eurasian temperate region, it absorbs about $-0.32 \pm 0.30\,\mathrm{Pg\,C\,yr^{-1}}$. The Eurasian boreal region is a weak carbon sink of $-0.07 \pm 0.49\,\mathrm{Pg\,C\,yr^{-1}}$. Inventory-based model estimates Eurasian temperate and boreal forests as a carbon sink of $-0.3 \pm 0.1\,\mathrm{Pg\,C\,yr^{-1}}$ (Goodale et al., 2002). However, Sarmiento et al. (2010) updates the carbon budget to be $-1.0 \pm 0.50\,\mathrm{Pg\,C\,yr^{-1}}$ for this region. Although it is hard to confirm the accuracy of our bottom-up simulation with the diverse results of previous studies, our estimation is not far from their results and seems to be reasonable. The Eurasian continent including Eurasian boreal, Eurasian temperate, tropical Asian and Europe areas sequestrate $-0.62 \pm 0.74\,\mathrm{Pg\,C\,yr^{-1}}$ and contributed to 30 % of the global terrestrial carbon sink. The third largest carbon sink is in South American tropics, which is around $-0.23 \pm 0.22\,\mathrm{Pg\,C\,yr^{-1}}$. Previous studies show that around $-0.5 \sim -0.8\,\mathrm{Pg\,C\,yr^{-1}}$ is taken up by old-grown tropical forest for the whole Amazonia (T. Baker et al., 2004; Phillips et al., 2008). Our result under-estimates the Amazonia forest carbon uptake. South American temperate is probably balanced in terrestrial carbon budget ($-0.02 \pm 0.23\,\mathrm{Pg\,C\,yr^{-1}}$). Its uncertainty is much larger than the magnitude of carbon sink. Therefore, it is hard to determine the sign of carbon budget in South American temperate region. North and South Africa play different

ACPD
14, 22587–22638, 2014

roles in the global carbon cycle. The northern part releases $0.05 \pm 0.28\,\mathrm{Pg\,C\,yr^{-1}}$, while the southern part absorbs $-0.10 \pm 0.23\,\mathrm{Pg\,C\,yr^{-1}}$. The Africa continent plays a limited role in controlling the global terrestrial carbon budget, since the Northern Africa carbon release compensates the carbon uptake in South Africa. Africa old-grown tropic forest is demonstrated to be a carbon sink of $-0.15 \sim -0.43\,\mathrm{Pg\,C\,yr^{-1}}$ (Lewis et al., 2009). Including both forest and savanna, Ciais et al. (2009) arrives at an estimation of $-0.28\,\mathrm{Pg\,C\,yr^{-1}}$ carbon sink. Our estimation seems to be low, thus warranted further attention in future analyses.

We aggregate the simulated global terrestrial ecosystem carbon budgets according to eight basic plant function types. Figure 6 shows the mean and uncertainty of the net ecosystem carbon fluxes for each PFT. The largest carbon absorption happens in forests, including boreal, temperate coniferous, temperate deciduous and tropical forests. Forests cover roughly 30 % of the land surface and could take up a substantial amount of atmospheric carbon with an annual uptake rate around $2.6\,\mathrm{Pg\,C\,yr^{-1}}$ in the 1990s (Bonan, 2008). The importance of forests in the global carbon budget is confirmed, although their result is larger than our estimation of $0.9\,\mathrm{Pg\,C\,yr^{-1}}$ carbon uptakes in 2003. The largest discrepancy is from tropical forest carbon uptake rate. The tropical forest annual carbon uptake rate is around $200\,\mathrm{g\,C\,m^{-2}\,yr^{-1}}$ in this study, while it is as large as $400\,\mathrm{g\,C\,m^{-2}\,yr^{-1}}$ based on Bonan (2008). The tundra and xeric woodland ecosystems are two weak carbon sinks. For tundra ecosystems, photosynthetic carbon production is strongly limited by low air temperate and is also influenced by the limited photosynthetic active radiation due to the short day length (McGuire et al., 2012; Sitch et al., 2007). For xeric woodland, the ecosystem usually experiences water limitation due to the low precipitation rate (Litvak et al., 2010). Therefore, it was reasonable to see that the magnitudes of carbon sink in tundra and xeric woodland ecosystem are much lower than forest ecosystems. Grassland and shrubland are possible weak carbon sources or even played a neutral role in the global terrestrial carbon cycle. Their uncertainties are generally larger than their mean values. It is hard to even determine the sign of the carbon budgets for these two plant function types.

ACPD
14, 22587–22638, 2014

In summary, our bottom-up results tend to overestimate terrestrial carbon uptake in North America and underestimate carbon sequestration rate in Amazonia and Africa. That is probably resulted from the plant functional type based scaling-up method, even though the method has been widely used in large-scale simulations. The AmeriFlux network provides useful information to constrain the carbon dynamics in biogeochemistry models, but the improvements are usually limited at site levels. It is problematic to scale up site-level calibrated model to a large region with a simple model extrapolation based on plant functional type (M. Chen and Zhuang, 2012). That is because the spatial heterogeneity of the same type of plant function is potentially large and is not well represented in the large-scale extrapolation (Zhu and Zhuang, 2013a). Therefore, the global carbon budgets simulated by the bottom-up biogeochemistry model warrant further refinement. Next we use an atmospheric transport model and CO_2 concentration data to further constrain the bottom-up approach estimated global carbon budgets.

3.2 Atmospheric CO_2 inverse modeling of surface carbon flux

We carry out two experiments of atmospheric CO_2 inversions with TEM simulated NEP (in Sect. 3.1.2) and CASA modeled NEP ($-5.29\,\mathrm{Pg\,C\,yr^{-1}}$) as priors. The CO_2 concentration data from surface network and satellite mid-troposphere retrievals are assimilated into GEOS-Chem to infer the magnitude and uncertainty of the terrestrial carbon budgets. We compare our estimations with previous work on atmospheric CO_2 inversions to explore the potential improvements or deficiencies of our results. Then we evaluate our posterior estimations of terrestrial ecosystem carbon budgets by comparing our modeled and observed atmospheric CO_2 concentrations time series at several representative inland sites from different continents. Hereafter, "GC-TEM" denotes GEOS-Chem inversion with TEM NEP prior; "GC-CASA" denotes GEOS-Chem inversion with CASA NEP prior.

ACPD
14, 22587–22638, 2014

3.2.1 Ecosystem carbon budgets constrained with CO_2 concentration data

Globally, GC-TEM estimates the terrestrial ecosystems as a carbon sink of $-2.47 \pm 0.98\,Pg\,C\,yr^{-1}$. Compared with the TEM NEP prior, the global terrestrial carbon budget is enhanced by 25 %. GC-CASA estimates the terrestrial ecosystems as a strong carbon sink as large as $-4.45 \pm 2.66\,Pg\,C\,yr^{-1}$, which differs from the he CASA NEP prior by $0.84\,Pg\,C\,yr^{-1}$. The results imply that TEM tends to underestimate NEP while CASA might greatly overestimate it. By assimilating atmospheric CO_2 concentration data, both inversions are able to approach more reasonable estimations of NEP. However, there still exists a large discrepancy between the two inversions. That is because the posterior estimation is not constrained by data only. Prior knowledge also plays an important role in determining the posterior (Kaminski and Heimann, 2001). Since our priors are largely different (TEM $-1.97\,Pg\,C\,yr^{-1}$ vs. CASA $-5.29\,Pg\,C\,yr^{-1}$), we expect to see that the posterior NEP discrepancy of the two inversions diminishes to some degree rather than completely vanishes. The recent CO_2 inversions inter-comparison study (Peylin et al., 2013) indicates that the mean of net carbon budget over land during 2001–2004 is $-1.32 \pm 0.39\,Pg\,C\,yr^{-1}$. Considering that roughly $1.5\,Pg\,C\,yr^{-1}$ are released due to land-use and land-cover change (Canadell et al., 2007; Le Quéréet al., 2009), the net terrestrial carbon budget should be around $-2.82\,Pg\,C\,yr^{-1}$. It agrees reasonably well with our GC-TEM estimation.

In terms of regional terrestrial carbon budgets, we compare our inversions with five other inversions from Integrated Carbon Observation System (ICOS) project (www.carboscope.eu). Table 4 summarizes their posteriors mean fluxes in 2003 at 11 predefined TransCom land regions. It also includes the GC-TEM and GC-CASA inversions. The five inversions estimate terrestrial ecosystem as a carbon sink ranging from -0.78 (Lsce_an_v2.1) to $-3.17\,Pg\,C\,yr^{-1}$ (Jena_s99_v3.3). It is hard to directly compare our estimation with any of theirs. Therefore, we average the regional fluxes for the five CarboScope inversions (Table 4). The largest departure between GC-TEM and GC-CASA is in the area of South Africa. GC-CASA indicates South Africa to be a strong

ACPD
14, 22587–22638, 2014

sink of atmospheric carbon ($-1.0\,Pg\,C\,yr^{-1}$), while GC-TEM estimates it as a weak sink around $-0.1\,Pg\,C\,yr^{-1}$. Two of the five CarboScope inversions indicate South Africa as a week carbon source (Jena_s96_v3.3 and Jena_s99_v3.3), but the ensembles mean of the five inversions identifies this region to be a weak carbon source ($0.16\,Pg\,C\,yr^{-1}$) with a large uncertainty ($0.28\,Pg\,C\,yr^{-1}$). As a result, the GC-TEM posterior in South Africa seems more reasonable than GC-CASA.

Large differences are also found in South America tropics among CarboScope ensemble mean (nearly neutral with only $0.022\,Pg\,C\,yr^{-1}$), GC-TEM (carbon sink with $-0.24\,Pg\,C\,yr^{-1}$) and GC-CASA (carbon source with $0.62\,Pg\,C\,yr^{-1}$). The tropics are among the most uncertain regions in the global carbon cycle, due to the scarcity of CO_2 observational network in this area (Gurney et al., 2002). The basic question that the tropics act as carbon sources or sinks is still intriguing and frequently revisited. Previously, it is thought that growth rate of the old-grown forest in South America tropics are quite limited. The old forests might cease to sequestrate atmospheric carbon due to their low carbon use efficiency (Chambers et al., 2004). Recently, however, more and more studies demonstrate that tropical forests are continuously assimilating atmospheric carbon and act as carbon sinks (Luyssaert et al., 2008; Stephens et al., 2007). For example, Stephen et al. (2008) infers the tropics to be a weak source of atmospheric carbon ($0.1\,Pg\,C\,yr^{-1}$), by analyzing vertical atmospheric CO_2 profiles. Their work concludes that after subtracting land-use and land-cover change induced carbon emissions in the tropics, the tropical lands are probably carbon sinks. It supports our estimation from GC-TEM in the South America tropical regions.

Major differences between GC-TEM and GC-CASA also exist in two other regions: south America temperate and Europe. In South America temperate region, GC-TEM generally agrees with the CarboScope ensemble mean and identifies this region as a weak carbon source ($0.0056\,Pg\,C\,yr^{-1}$ and $0.044\,Pg\,C\,yr^{-1}$, respectively). In contrast, GC-CASA identifies it as a strong carbon sink with $-0.65\,Pg\,C\,yr^{-1}$. And both CarboScope ensemble mean and GC-TEM estimate a carbon sink around $-0.3\,Pg\,C\,yr^{-1}$ in

ACPD
14, 22587–22638, 2014

Europe region. However, the carbon sink estimated by GC-CASA is two times larger than GC-TEM.

We conclude that GC-TEM posterior terrestrial carbon budgets are more consistent with previous studies and empirical knowledge than GC-CASA. Using the same observational datasets and transport model could result in significantly different posterior due to the differences in prior information. A reliable prior achieved by synthesizing biogeochemistry models and observed net carbon flux data is desirable for robust estimations of the global terrestrial carbon budget.

3.2.2 Evaluation with GLOBALVIEW-CO2

Six GLOBALVIEW-CO2 sites are reserved for validation purpose (Table 3). They measure CO_2 concentrations time series at inland locations, which are used as proxies to evaluate sub-continental carbon dynamics. Figure 7 compares the GC-TEM and GC-CASA simulated atmospheric CO_2 concentrations against observations in 2003. The model-data misfits are measured by Root Mean Square Error (RMSE). At all the six locations, the GC-TEM RMSEs are smaller than those of GC-CASA. The scatter plots shows that GC-CASA under-estimates CO_2 concentrations at Australia, South America temperate and North Africa regions. It overestimates CO_2 concentrations in Europe area. In North America temperate and Asia temperate regions, it either overestimates or underestimates CO_2 concentrations depending on the time period of a year.

Although GC-TEM performs reasonably well, RMSEs are relatively large in Europe (4.98 ppm) and North America temperate regions (4.11 ppm). GC-TEM overestimates atmospheric CO_2 concentrations at the Europe site. It indicates that the terrestrial carbon sink in Europe might be underestimated in GC-TEM experiments, if we suppose other background carbon fluxes (e.g. fossil fuel emissions) are correct. GC-TEM underestimates atmospheric CO_2 concentrations at the US site. Similarly, it implies that the terrestrial carbon uptake in North America temperate region might be overestimated in GC-TEM.

ACPD
14, 22587–22638, 2014

3.2.3 Evaluation with CONTRAIL CO

2

Figure 8 depicts the monthly averages of CONTRIAL CO2 concentration observations in three latitude bins (30° N–10° N, 10° N–10° S, 10° S–30° S). GEOS-Chem posterior CO_2 concentration at CONTRAIL CO_2 sampling locations are also grouped into the three bins and compared with the observations. We find that the GC-TEM is superior to GC-CASA in reproducing the atmospheric CO_2 concentration. The RMSEs are 1.28, 1.16, 0.69 (ppm) between GC-TEM and CONTRAIL CO_2 for the three latitude bins, respectively. The RMSEs between GC-CASA and CONTRIAL CO_2, however, are as large as 2.19, 2.03, 2.34 (ppm). The GC-CASA tends to underestimate atmospheric CO_2 concentrations at all the northern subtropical, tropical and southern subtropical regions. It indicates that the magnitude of CO_2 sink into earth surface might be overestimated in GC-CASA.

Although GC-TEM performs relatively better than GC-CASA, it overestimates atmospheric CO_2 concentrations from April to July for tropical region and from May to June for northern subtropical region. For southern subtropical regions, the CO_2 concentrations are well reproduced by GC-TEM and they are contained within the CONTRIAL CO_2 uncertainty bounds. It implies that GC-TEM might have underestimated the land surface CO_2 sinks during April–July between 30° N and 10° S nearby CONTRAIL sampling paths.

4 Conclusions

In this study, we present a two-phase system combining the bottom-up and top-down approaches to estimate the global terrestrial carbon budgets. It consists of two phases, during which different types of carbon data are assimilated into the system to constrain the carbon budgets. During phase one, canopy level carbon flux data (AmeriFlux NEP) are fused into a terrestrial ecosystem model (TEM) to improve the model predictability

ACPD
14, 22587–22638, 2014

in carbon dynamics. Then the improved model is used to simulate large-scale carbon budgets and associated uncertainties to serve as prior for atmospheric CO_2 inversion. During phase two, we use a 4-D variational approach to assimilate multiple CO_2 concentration datasets (GLOBALVIEW-CO2 and AIRS) into an atmospheric transport model (GEOS-Chem) and to infer the magnitude and spatial distribution of terrestrial ecosystem carbon budgets.

We find that the terrestrial ecosystem acted as a carbon sink of $-2.47 \pm 0.98\,\mathrm{Pg\,C\,yr^{-1}}$ in 2003. Most of the terrestrial sinks are attributed to North America temperate, Europe and Eurasia temperate regions. South America temperate and North Africa act as weak sources of atmospheric carbon with a total carbon source of $0.03\,\mathrm{Pg\,C\,yr^{-1}}$ in 2003. North America boreal, Eurasia boreal and Australia play similar roles in the global carbon cycle. They absorb a roughly equal amount of atmospheric carbon ($-0.15\,\mathrm{Pg\,C\,yr^{-1}}$). The tropical South America and tropical Asia totally sequestrate $-0.27\,\mathrm{Pg\,C\,yr^{-1}}$.

Our coupled top-down and bottom-up approach is effective for inversing fluxes, especially for areas that CO_2 concentrations are not well observed by the CO_2 network (Gurney et al., 2008; Kaminski and Heimann, 2001). Another advantage of our study is that CO_2 observations from different vertical levels are assimilated into the system. Although surface CO_2 networks are generally sparse, they are complementary with satellite CO_2 data. The high sensitivity of near surface CO_2 concentrations to surface carbon dynamics together with the large horizontal coverage of satellite retrievals could benefit the estimations of global terrestrial carbon fluxes (Nassar et al., 2011). In this study, we assimilate both the GLOBALVIEW-CO2 surface CO_2 and AIRS mid-troposphereCO_2. The results agree well with recent inter-comparison studies (Peylin et al., 2013) and CarboScope ensemble inversions.

Our study has several limitations. First, the uncertainties come from TEM scaling up method. In this study we adopt a classical scale-up method (model calibrated at site level and scaling up to a region based on vegetation type), which has been widely used in previous studies (Melillo et al., 1993; Zhuang et al., 2010). However, although the

ACPD
14, 22587–22638, 2014

model is carefully trained and could reasonably reproduce observed terrestrial ecosystem carbon dynamics at representative sites for various plant functional types, the spatial heterogeneities could be large within the same plant functional type (M. Chen and Zhuang, 2012; Zhu and Zhuang, 2013a). Even within the same plant functional type, species-level differences might also lead to different estimates of carbon dynamics (He et al., 2013). Another limitation is that we do not consider the atmospheric CO_2 transport error while we consider the uncertainties in terrestrial carbon budgets. The mid-troposphere CO_2 concentrations are affected by not only surface sources; but also large-scale transport (Chahine et al., 2008) has errors and uncertainties, which should be considered in future analysis with our coupled bottom-up and top-down approach.

Acknowledgements. We thank the eddy flux network principal investigators for providing carbon flux data. We thank AIRS CO2 and Globalview-CO2 groups for providing atmospheric CO_2 concentration data. We also thank CarboScope for contributing inversions results for our intercomparison purpose. This research is funded by NASA Land Use and Land Cover Change program (NASA-NNX09A126G), Department of Energy (DE-FG02-08ER64599), National Science Foundation (NSF-102891 and NSF-0919331), NSF Carbon and Water in the Earth Program (NSF-0630319) and NSF CDI Type II project (IIS-1028291).

Appendix A: TEM model description

The Terrestrial Ecosystem Model (TEM) solves a set of ordinary differential equations (ODEs) to calculate the changes of five biogeochemical pools including vegetation carbon (C_V), soil carbon (C_S), vegetation nitrogen (N_V), soil organic nitrogen (N_S) and soil available inorganic nitrogen (N_{AV}) at a monthly time step. The model is driven with spatially explicit data of climate (precipitation, radiation, air temperature) and elevation, soil type and vegetation cover.

The net carbon budget or net ecosystem production (NEP) is estimated as the balance between photosynthesis and ecosystem respiration including autotrophic respi-

ACPD
14, 22587–22638, 2014

ration (R_A) and heterotrophic respiration (R_H):

$$NEP = GPP - R_A - R_H \quad (A1)$$

where the gross primary production (GPP) is calculated as:

$$GPP = C_{max} \cdot f(PAR) \cdot f(T) \cdot f(C_a, C_v) \cdot f(phenology) \cdot f(others) \quad (A2)$$

where C_{max} is the maximum carbon assimilation capacity of plants. The maximum capacity is constrained under various environmental and ecological conditions, which are represented by function $f(\cdot)$. $f(PAR)$ and $f(T)$ are scalar factors that impose photosynthetic active radiation (PAR) and temperature limitations on plant photosynthesis. $f(C_a, C_v)$ represents the atmospheric CO_2 concentrations (C_a) effect and canopy conductance (C_v) effect. $f(phenology)$ considers the influence of the leaf area dynamics on photosynthesis. $f(others)$ includes various other constraints that either have relatively small effects on photosynthesis or are not directly related with photosynthesis (e.g., nutrient supply). Further details about the scalar factor formulations could be found in (Raich et al., 1991; McGuire et al., 1992).

Autotrophic respiration (R_A) is calculated as a summation of plant maintenance respiration (R_m) and plant growth respiration (R_g). The growth respiration is assumed to be 20 % of the difference between plant photosynthesis and maintenance respiration, where R_m is modeled with a classic Q10 relationship:

$$R_m = K_R \cdot C_V \cdot f(RAQ10) \quad (A3)$$

$$R_g = 20\% \cdot (GPP - R_m) \quad (A4)$$

$$R_A = R_m + R_g \quad (A5)$$

where K_R and C_V are autotrophic respiration rate at reference temperature (10 °C) and vegetation carbon biomass. $f(RAQ10)$ represents the dependence of autotrophic respiration on air temperature. Similar to plant maintenance respiration, the terrestrial

ACPD
14, 22587–22638, 2014

ecosystem heterotrophic respiration (R_H) is modeled with:

$$R_H = K_D \cdot C_S \cdot f(\mathrm{RHQ10}) \cdot \mathrm{MOIST} \quad \text{(A6)}$$

here K_D and C_S are heterotrophic respiration at reference temperature and soil carbon pool size. f(RHQ10) and MOIST are effects of soil temperature and moisture on R_H.

References

Andres, R. J., Gregg, J. S., Losey, L., Marland, G., and Boden, T. A.: Monthly, global emissions of carbon dioxide from fossil fuel consumption, Tellus B, 63, 309–327, 2011.

Aumann, H. H., Chahine, M. T., Gautier, C., Goldberg, M. D., Kalnay, E., McMillin, L. M., Revercomb, H., Rosenkranz, P. W., Smith, W. L., and Staelin, D. H.: AIRS/AMSU/HSB on the Aqua mission: design, science objectives, data products, and processing systems, IEEE T. Geosci. Remote, 41, 253–264, 2003.

Baker, D., Law, R., Gurney, K., Rayner, P., Peylin, P., Denning, A., Bousquet, P., Bruhwiler, L., Chen, Y. H., and Ciais, P.: TransCom 3 inversion intercomparison: impact of transport model errors on the interannual variability of regional CO_2 fluxes, 1988–2003, Global Biogeochem. Cy., 20, GB1002, doi:10.1029/2004GB002439, 2006.

Baker, T., Phillips, O. L., Malhi, Y., Almeida, S., Arroyo, L., Di Fiore, A., Erwin, T., Higuchi, N., Killeen, T. J., and Laurance, S. G.: Increasing biomass in Amazonian forest plots, Philos. T. Roy. Soc. Lond. B, 359, 353–365, 2004.

Baldocchi, D.: Assessing the eddy covariance technique for evaluating carbon dioxide exchange rates of ecosystems: past, present and future, Glob. Change Biol., 9, 479–492, 2003.

Baldocchi, D.: TURNER REVIEW No. 15. 'Breathing' of the terrestrial biosphere: lessons learned from a global network of carbon dioxide flux measurement systems, Austral. J. Bot., 56, 1–26, 2008.

Baldocchi, D., Falge, E., Gu, L., Olson, R., Hollinger, D., Running, S., Anthoni, P., Bernhofer, C., Davis, K., and Evans, R.: FLUXNET: a new tool to study the temporal and spatial variability of ecosystem-scale carbon dioxide, water vapor, and energy flux densities, B. Am. Meteorol. Soc., 82, 2415–2434, 2001.

Basu, S., Guerlet, S., Butz, A., Houweling, S., Hasekamp, O., Aben, I., Krummel, P., Steele, P., Langenfelds, R., Torn, M., Biraud, S., Stephens, B., Andrews, A., and Worthy, D.: Global

ACPD
14, 22587–22638, 2014

CO_2 fluxes estimated from GOSAT retrievals of total column CO_2, Atmos. Chem. Phys., 13, 8695–8717, doi:10.5194/acp-13-8695-2013, 2013.

Bey, I., Jacob, D. J., Yantosca, R. M., Logan, J. A., Field, B. D., Fiore, A. M., Li, Q., Liu, H. Y., Mickley, L. J., and Schultz, M. G.: Global modeling of tropospheric chemistry with assimilated meteorology: model description and evaluation, J. Geophys. Res., 106, 23073–23023, 23095, 2001.

Bloom, S., Da Silva, A., Dee, D., Bosilovich, M., Chern, J., Pawson, S., Schubert, S., Sienkiewicz, M., Stajner, I., and Tan, W.: Documentation and validation of the Goddard Earth Observing System (GEOS) data assimilation system – Version 4, NASA Tech. Memo, Greenbelt, MD, USA, 2005.

Bonan, G. B.: Forests and climate change: forcings, feedbacks, and the climate benefits of forests, Science, 320, 1444–1449, 2008.

Broyden, C. G.: The convergence of a class of double-rank minimization algorithms 1. general considerations, IMA J. Appl. Math., 6, 76–90, 1970.

Brunke, E.-G., Labuschagne, C., Parker, B., Scheel, H., and Whittlestone, S.: Baseline air mass selection at Cape Point, South Africa: application of ^{222}Rn and other filter criteria to CO_2, Atmos. Environ., 38, 5693–5702, 2004.

Byrd, R. H., Lu, P., Nocedal, J., and Zhu, C.: A limited memory algorithm for bound constrained optimization, SIAM J. Sci. Comput., 16, 1190–1208, 1995.

Canadell, J. G., Le Quéré, C., Raupach, M. R., Field, C. B., Buitenhuis, E. T., Ciais, P., Conway, T. J., Gillett, N. P., Houghton, R., and Marland, G.: Contributions to accelerating atmospheric CO_2 growth from economic activity, carbon intensity, and efficiency of natural sinks, P. Natl. Acad. Sci. USA, 104, 18866–18870, 2007.

Chahine, M., Barnet, C., Olsen, E., Chen, L., and Maddy, E.: On the determination of atmospheric minor gases by the method of vanishing partial derivatives with application to CO_2, Geophys. Res. Lett., 32, L22803, doi:10.1029/2005GL024165, 2005.

Chahine, M., Chen, L., Dimotakis, P., Jiang, X., Li, Q., Olsen, E. T., Pagano, T., Randerson, J., and Yung, Y. L.: Satellite remote sounding of mid-tropospheric CO_2, Geophys. Res. Lett., 35, L17807, 2008.

Chambers, J. Q., Tribuzy, E. S., Toledo, L. C., Crispim, B. F., Higuchi, N., Santos, J. d., Araújo, A. C., Kruijt, B., Nobre, A. D., and Trumbore, S. E.: Respiration from a tropical forest ecosystem: partitioning of sources and low carbon use efficiency, Ecol. Appl., 14, 72–88, 2004.

ACPD
14, 22587–22638, 2014

Chédin, A., Serrar, S., Scott, N., Crevoisier, C., and Armante, R.: First global measurement of midtropospheric CO_2 from NOAA polar satellites: tropical zone, J. Geophys. Res., 108, 4581, doi:10.1029/2003JD003439, 2003.

Chen, M. and Zhuang, Q.: Spatially explicit parameterization of a terrestrial ecosystem model and its application to the quantification of carbon dynamics of forest ecosystems in the conterminous United States, Earth Interact., 16, 1–22, 2012.

Chen, Z., Yu, G., Ge, J., Sun, X., Hirano, T., Saigusa, N., Wang, Q., Zhu, X., Zhang, Y., and Zhang, J.: Temperature and precipitation control of the spatial variation of terrestrial ecosystem carbon exchange in the Asian region, Agr. Forest Meteorol., 182, 266–276, 2013.

Chevallier, F. and O'Dell, C. W.: Error statistics of Bayesian CO_2 flux inversion schemes as seen from GOSAT, Geophys. Res. Lett., 40, 1252–1256, 2013.

Chevallier, F., Engelen, R. J., Carouge, C., Conway, T. J., Peylin, P., Pickett-Heaps, C., Ramonet, M., Rayner, P. J., and Xueref-Remy, I.: AIRS-based vs. flask-based estimation of carbon surface fluxes, J. Geophys. Res.-Atmos., 114, D20303, doi:10.1029/2009JD012311, 2009.

Chevallier, F., Wang, T., Ciais, P., Maignan, F., Bocquet, M., Altaf Arain, M., Cescatti, A., Chen, J., Dolman, A. J., and Law, B. E.: What eddy-covariance measurements tell us about prior land flux errors in CO_2-flux inversion schemes, Global Biogeochem. Cy., 26, GB1021, doi:10.1029/2010GB003974, 2012.

Ciais, P., Piao, S.-L., Cadule, P., Friedlingstein, P., and Chédin, A.: Variability and recent trends in the African terrestrial carbon balance, Biogeosciences, 6, 1935–1948, doi:10.5194/bg-6-1935-2009, 2009.

Corbett, J. J. and Koehler, H. W.: Updated emissions from ocean shipping, J. Geophys. Res.-Atmos., 108, 4650, doi:10.1029/2003JD003751, 2003.

Dargaville, R., Baker, D., Rödenbeck, C., Rayner, P., and Ciais, P.: Estimating high latitude carbon fluxes with inversions of atmospheric CO_2, Mitig. Adapt. Strat. Glob. Change, 11, 769–782, 2006.

Deng, F., Jones, D. B. A., Henze, D. K., Bousserez, N., Bowman, K. W., Fisher, J. B., Nassar, R., O'Dell, C., Wunch, D., Wennberg, P. O., Kort, E. A., Wofsy, S. C., Blumenstock, T., Deutscher, N. M., Griffith, D. W. T., Hase, F., Heikkinen, P., Sherlock, V., Strong, K., Sussmann, R., and Warneke, T.: Inferring regional sources and sinks of atmospheric CO_2 from GOSAT XCO_2 data, Atmos. Chem. Phys., 14, 3703–3727, doi:10.5194/acp-14-3703-2014, 2014.

ACPD
14, 22587–22638, 2014

Forster, P., Ramaswamy, V., Artaxo, P., Berntsen, T., Betts, R., Fahey, D. W., Haywood, J., Lean, J., Lowe, D. C., and Myhre, G.: Changes in atmospheric constituents and in radiative forcing, Climate Change, 129–234, Cambridge University Press, Cambridge, UK, 2007.

Friedl, R.: Atmospheric effects of subsonic aircraft: interim assessment report of the advanced subsonic technology program, NASA Reference Publication 1400, NASA, Washington D. C., USA, 1997.

Giering, R. and Kaminski, T.: Recipes for adjoint code construction, ACM Trans. Math. Softw. (TOMS), 24, 437–474, 1998.

Globalview-CO2: Cooperative Global Atmospheric Data Integration Project, Multi-laboratory compilation of synchronized and gap-filled atmospheric carbon dioxide records for the period 1979–2012 (obspack_co2_1_GLOBALVIEW-CO2_2013_v1.0.4_2013–12-23), NOAA Global Monitoring Division: Boulder, Colorado, USA, 2013.

Gloor, M., Fan, S. M., Pacala, S., and Sarmiento, J.: Optimal sampling of the atmosphere for purpose of inverse modeling: a model study, Global Biogeochem. Cy., 14, 407–428, 2000.

Goodale, C. L., Apps, M. J., Birdsey, R. A., Field, C. B., Heath, L. S., Houghton, R. A., Jenkins, J. C., Kohlmaier, G. H., Kurz, W., and Liu, S.: Forest carbon sinks in the Northern Hemisphere, Ecol. Appl., 12, 891–899, 2002.

Gurney, K., Law, R. M., Denning, A. S., Rayner, P. J., Baker, D., Bousquet, P., Bruhwiler, L., Chen, Y.-H., Ciais, P., and Fan, S.: Towards robust regional estimates of CO_2 sources and sinks using atmospheric transport models, Nature, 415, 626–630, 2002.

Gurney, K., Law, R. M., Denning, A. S., Rayner, P. J., Pak, B. C., Baker, D., Bousquet, P., Bruhwiler, L., Chen, Y. H., and Ciais, P.: Transcom 3 inversion intercomparison: model mean results for the estimation of seasonal carbon sources and sinks, Global Biogeochem. Cy., 18, GB1010, doi:10.1029/2003GB002111, 2004.

Gurney, K., Baker, D., Rayner, P., and Denning, S.: Interannual variations in continental-scale net carbon exchange and sensitivity to observing networks estimated from atmospheric CO_2 inversions for the period 1980 to 2005, Global Biogeochem. Cy., 22, GB3025, doi:10.1029/2007GB003082, 2008.

He, Y., Zhuang, Q., McGuire, A. D., Liu, Y., and Chen, M.: Alternative ways of using field-based estimates to calibrate ecosystem models and their implications for carbon cycle studies, J. Geophys. Res., 118, 983–993, doi:10.1002/jgrg.20080, 2013.

ACPD
14, 22587–22638, 2014

Heinsch, F., Heilman, J., McInnes, K., Cobos, D., Zuberer, D., and Roelke, D.: Carbon dioxide exchange in a high marsh on the Texas Gulf Coast: effects of freshwater availability, Agr. Forest Meteorol., 125, 159–172, 2004.
Henze, D. K., Hakami, A., and Seinfeld, J. H.: Development of the adjoint of GEOS-Chem, Atmos. Chem. Phys., 7, 2413–2433, doi:10.5194/acp-7-2413-2007, 2007.
Houghton, R. A.: Revised estimates of the annual net flux of carbon to the atmosphere from changes in land use and land management 1850–2000, Tellus B, 55, 378–390, 2003.
Houghton, R. A.: Balancing the global carbon budget, Annu. Rev. Earth Planet. Sci., 35, 313–347, 2007.
Houweling, S., Breon, F.-M., Aben, I., Rödenbeck, C., Gloor, M., Heimann, M., and Ciais, P.: Inverse modeling of CO_2 sources and sinks using satellite data: a synthetic inter-comparison of measurement techniques and their performance as a function of space and time, Atmos. Chem. Phys., 4, 523–538, doi:10.5194/acp-4-523-2004, 2004.
Jacobson, A. R., Mikaloff Fletcher, S. E., Gruber, N., Sarmiento, J. L., and Gloor, M.: A joint atmosphere–ocean inversion for surface fluxes of carbon dioxide: 1. Methods and global-scale fluxes, Global Biogeochem. Cy., 21, GB1019, doi:10.1029/2005GB002556, 2007a.
Jacobson, A. R., Fletcher, S. E. M., Gruber, N., Sarmiento, J. L., and Gloor, M.: A joint atmosphere–ocean inversion for surface fluxes of carbon dioxide: 2. Regional results, Global Biogeochem. Cy., 21, GB1020, doi:10.1029/2006GB002703, 2007b.
Janssens, I. A., Freibauer, A., Schlamadinger, B., Ceulemans, R., Ciais, P., Dolman, A. J., Heimann, M., Nabuurs, G.-J., Smith, P., Valentini, R., and Schulze, E.-D.: The carbon budget of terrestrial ecosystems at country-scale – a European case study, Biogeosciences, 2, 15–26, doi:10.5194/bg-2-15-2005, 2005.
Jung, M., Reichstein, M., Margolis, H. A., Cescatti, A., Richardson, A. D., Arain, M. A., Arneth, A., Bernhofer, C., Bonal, D., and Chen, J.: Global patterns of land–atmosphere fluxes of carbon dioxide, latent heat, and sensible heat derived from eddy covariance, satellite, and meteorological observations, J. Geophys. Res.: Biogeosciences, 26, G00J07, doi:10.1029/2010JG001566, 2011.
Kaminski, T. and Heimann, M.: Inverse modeling of atmospheric carbon dioxide fluxes, Science, 294, 259–259, 2001.
Kaul, M., Dadhwal, V., and Mohren, G.: Land use change and net C flux in Indian forests, Forest Ecol. Manage., 258, 100–108, 2009.

ACPD
14, 22587–22638, 2014

Knorr, W. and Heimann, M.: Uncertainties in global terrestrial biosphere modeling: 1. A comprehensive sensitivity analysis with a new photosynthesis and energy balance scheme, Global Biogeochem. Cy., 15, 207–225, 2001.

Knorr, W. and Kattge, J.: Inversion of terrestrial ecosystem model parameter values against eddy covariance measurements by Monte Carlo sampling, Glob. Change Biol., 11, 1333–1351, 2005.

Kopacz, M., Jacob, D., Henze, D., Heald, C., Streets, D., and Zhang, Q.: A comparison of analytical and adjoint Bayesian inversion methods for constraining Asian sources of CO using satellite (MOPITT) measurements of CO columns, paper presented at AGU Fall Meeting Abstracts, 1, 875, December 2006, San Francisco, CA, USA, 2006.

Kuppel, S., Peylin, P., Chevallier, F., Bacour, C., Maignan, F., and Richardson, A. D.: Constraining a global ecosystem model with multi-site eddy-covariance data, Biogeosciences, 9, 3757–3776, doi:10.5194/bg-9-3757-2012, 2012.

Le Quéré, C., Raupach, M. R., Canadell, J. G., and Marland, G.: Trends in the sources and sinks of carbon dioxide, Nat. Geosci., 2, 831–836, 2009.

Le Quéré, C., Andres, R. J., Boden, T., Conway, T., Houghton, R. A., House, J. I., Marland, G., Peters, G. P., van der Werf, G. R., Ahlström, A., Andrew, R. M., Bopp, L., Canadell, J. G., Ciais, P., Doney, S. C., Enright, C., Friedlingstein, P., Huntingford, C., Jain, A. K., Jourdain, C., Kato, E., Keeling, R. F., Klein Goldewijk, K., Levis, S., Levy, P., Lomas, M., Poulter, B., Raupach, M. R., Schwinger, J., Sitch, S., Stocker, B. D., Viovy, N., Zaehle, S., and Zeng, N.: The global carbon budget 1959–2011, Earth Syst. Sci. Data, 5, 165–185, doi:10.5194/essd-5-165-2013, 2013.

Lewis, S. L., Lopez-Gonzalez, G., Sonké, B., Affum-Baffoe, K., Baker, T. R., Ojo, L. O., Phillips, O. L., Reitsma, J. M., White, L., and Comiskey, J. A.: Increasing carbon storage in intact African tropical forests, Nature, 457, 1003–1006, 2009.

Litvak, M. E., Schwinning, S., and Heilman, J. L.: Woody plant rooting depth and ecosystem function of savannas: a case study from the Edwards Plateau Karst, Texas, Ecosyst. Funct. Savannas: Meas. Model. Landsc. Glob. Scales, edited by: Hill, M. J. and Hanan, N. P., chapter 6, 2010.

Luo, Y., White, L. W., Canadell, J. G., DeLucia, E. H., Ellsworth, D. S., Finzi, A., Lichter, J., and Schlesinger, W. H.: Sustainability of terrestrial carbon sequestration: a case study in Duke Forest with inversion approach, Global Biogeochem. Cy., 17, 1021, doi:10.1029/2002GB001923, 2003.

ACPD
14, 22587–22638, 2014

Luyssaert, S., Schulze, E.-D., Börner, A., Knohl, A., Hessenmöller, D., Law, B. E., Ciais, P., and Grace, J.: Old-growth forests as global carbon sinks, Nature, 455, 213–215, 2008.

Machida, T., Tohjima, Y., Katsumata, K., and Mukai, H.: A new CO_2 calibration scale based on gravimetric one-step dilution cylinders in National Institute for Environmental Studies-NIES 09 CO2 scale, GAW Report, 194, 114–119, 2011.

Maddy, E., Barnet, C., Goldberg, M., Sweeney, C., and Liu, X.: CO_2 retrievals from the Atmospheric Infrared Sounder: methodology and validation, J. Geophys. Res.-Atmos., 113, D11301, doi:10.1029/2007JD009402, 2008.

Marland, G., Boden, T. A., Andres, R. J., Brenkert, A., and Johnston, C.: Global, regional, and national fossil fuel CO_2 emissions, Trends, Oak Ridge National Laboratory, US Department of Energy, Oak Ridge, Tenn., USA, 2003, 34–43, 2003.

Masarie, K. A. and Tans, P. P.: Extension and integration of atmospheric carbon dioxide data into a globally consistent measurement record, J. Geophys. Res.-Atmos., 100, 11593–11610, 1995.

Matsueda, H., Machida, T., Sawa, Y., Nakagawa, Y., Hirotani, K., Ikeda, H., Kondo, N., and Goto, K.: Evaluation of atmospheric CO_2 measurements from new flask air sampling of JAL airliner observations, Paper. Meteorol. Geophys., 59, 1–17, 2008.

McGuire, A. D., Melillo, J., Joyce, L., Kicklighter, D., Grace, A., Moore, B., and Vorosmarty, C.: Interactions between carbon and nitrogen dynamics in estimating net primary productivity for potential vegetation in North America, Global Biogeochem. Cy., 6, 101–124, 1992.

McGuire, A. D., Christensen, T. R., Hayes, D., Heroult, A., Euskirchen, E., Kimball, J. S., Koven, C., Lafleur, P., Miller, P. A., Oechel, W., Peylin, P., Williams, M., and Yi, Y.: An assessment of the carbon balance of Arctic tundra: comparisons among observations, process models, and atmospheric inversions, Biogeosciences, 9, 3185–3204, doi:10.5194/bg-9-3185-2012, 2012.

McMillan, W., Barnet, C., Strow, L., Chahine, M., McCourt, M., Warner, J., Novelli, P., Korontzi, S., Maddy, E., and Datta, S.: Daily global maps of carbon monoxide from NASA's Atmospheric Infrared Sounder, Geophys. Res. Lett., 32, L11801, doi:10.1029/2004GL021821, 2005.

Medlyn, B. E., Robinson, A. P., Clement, R., and McMurtrie, R. E.: On the validation of models of forest CO_2 exchange using eddy covariance data: some perils and pitfalls, Tree Physiol., 25, 839–857, 2005.

ACPD
14, 22587–22638, 2014

Medvigy, D., Wofsy, S. C., Munger, J. W., and Moorcroft, P. R.: Responses of terrestrial ecosystems and carbon budgets to current and future environmental variability, P. Natl. Acad. Sci. USA, 107, 8275–8280, 2010.

Melillo, J. M., McGuire, A. D., Kicklighter, D. W., Moore, B., Vorosmarty, C. J., and Schloss, A. L.: Global climate change and terrestrial net primary production, Nature, 363, 234–240, 1993.

Monahan, K., Pan, L., McDonald, A., Bodeker, G., Wei, J., George, S., Barnet, C., and Maddy, E.: Validation of AIRS v4 ozone profiles in the UTLS using ozonesondes from Lauder, NZ and Boulder, USA, J. Geophys. Res., 112, D17304, doi:10.1029/2006JD008181, 2007.

Nassar, R., Jones, D. B. A., Suntharalingam, P., Chen, J. M., Andres, R. J., Wecht, K. J., Yantosca, R. M., Kulawik, S. S., Bowman, K. W., Worden, J. R., Machida, T., and Matsueda, H.: Modeling global atmospheric CO_2 with improved emission inventories and CO_2 production from the oxidation of other carbon species, Geosci. Model Dev., 3, 689–716, doi:10.5194/gmd-3-689-2010, 2010.

Nassar, R., Jones, D. B. A., Kulawik, S. S., Worden, J. R., Bowman, K. W., Andres, R. J., Suntharalingam, P., Chen, J. M., Brenninkmeijer, C. A. M., Schuck, T. J., Conway, T. J., and Worthy, D. E.: Inverse modeling of CO_2 sources and sinks using satellite observations of CO_2 from TES and surface flask measurements, Atmos. Chem. Phys., 11, 6029–6047, doi:10.5194/acp-11-6029-2011, 2011.

Olsen, E. T.: AIRS Version 5 Release Tropospheric CO_2 Products, Jet Propulsion Laboratory, California Institute of Technology, Pasadena, CA, 2009.

Pacala, S., R. Birdsey, S. Bridgham, R. Conant, K. Davis, B. Hales, R. Houghton, J. Jenkins, M. Johnston, G. Marland, K. Paustian, J. Caspersen, R. Socolow, R. Tol: The North American carbon budget past and present, in: The First State of the Carbon Cycle Report (SOCCR): The North American Carbon Budget and Implications for the Global Carbon Cycle, edited by: A. W. King, L. Dilling, G. P. Zimmerman, D. M. Fairman, R. A. Houghton, G. Marland, A. Z. Rose, T. J. Wilbanks, National Oceanic and Atmospheric Administration, National Climatic Data Center, Asheville, NC, USA, 2007,

Peters, W., Jacobson, A. R., Sweeney, C., Andrews, A. E., Conway, T. J., Masarie, K., Miller, J. B., Bruhwiler, L. M., Petron, G., and Hirsch, A. I.: An atmospheric perspective on North American carbon dioxide exchange: carbonTracker, P. Natl. Acad. Sci. USA, 104, 18925–18930, 2007.

ACPD
14, 22587–22638, 2014

Peylin, P., Baker, D., Sarmiento, J., Ciais, P., and Bousquet, P.: Influence of transport uncertainty on annual mean and seasonal inversions of atmospheric CO_2 data, J. Geophys. Res., 107, 4385, doi:10.1029/2001JD000857, 2002.

Peylin, P., Law, R. M., Gurney, K. R., Chevallier, F., Jacobson, A. R., Maki, T., Niwa, Y., Patra, P. K., Peters, W., Rayner, P. J., Rödenbeck, C., van der Laan-Luijkx, I. T., and Zhang, X.: Global atmospheric carbon budget: results from an ensemble of atmospheric CO_2 inversions, Biogeosciences, 10, 6699–6720, doi:10.5194/bg-10-6699-2013, 2013.

Phillips, O. L., Lewis, S. L., Baker, T. R., Chao, K.-J., and Higuchi, N.: The changing Amazon forest, Philos. T. R. Soc. B, 363, 1819–1827, 2008.

Piao, S., Fang, J., Ciais, P., Peylin, P., Huang, Y., Sitch, S., and Wang, T.: The carbon balance of terrestrial ecosystems in China, Nature, 458, 1009–1013, 2009.

Randerson, J., Chapin Iii, F. S., Harden, J., Neff, J., and Harmon, M.: Net ecosystem production: a comprehensive measure of net carbon accumulation by ecosystems, Ecol. Appl., 12, 937–947, 2002.

Raupach, M., Rayner, P., Barrett, D., DeFries, R., Heimann, M., Ojima, D., Quegan, S., and Schmullius, C.: Model–data synthesis in terrestrial carbon observation: methods, data requirements and data uncertainty specifications, Glob. Change Biol., 11, 378–397, 2005.

Rödenbeck, C., Houweling, S., Gloor, M., and Heimann, M.: Time-dependent atmospheric CO_2 inversions based on interannually varying tracer transport, Tellus B, 55, 488–497, 2003.

Sabine, C. L., Feely, R. A., Gruber, N., Key, R. M., Lee, K., Bullister, J. L., Wanninkhof, R., Wong, C., Wallace, D. W., and Tilbrook, B.: The oceanic sink for anthropogenic CO_2, Science, 305, 367–371, 2004.

Saeki, T., Maksyutov, S., Sasakawa, M., Machida, T., Arshinov, M., Tans, P., Conway, T., Saito, M., Valsala, V., and Oda, T.: Carbon flux estimation for Siberia by inverse modeling constrained by aircraft and tower CO_2 measurements, J. Geophys. Res.-Atmos., 118, 1100–1122, 2013.

Sarmiento, J. L., Gloor, M., Gruber, N., Beaulieu, C., Jacobson, A. R., Mikaloff Fletcher, S. E., Pacala, S., and Rodgers, K.: Trends and regional distributions of land and ocean carbon sinks, Biogeosciences, 7, 2351–2367, doi:10.5194/bg-7-2351-2010, 2010.

Schimel, D. S., House, J., Hibbard, K., Bousquet, P., Ciais, P., Peylin, P., Braswell, B. H., Apps, M. J., Baker, D., and Bondeau, A.: Recent patterns and mechanisms of carbon exchange by terrestrial ecosystems, Nature, 414, 169–172, 2001.

ACPD
14, 22587–22638, 2014

Schmid, H.: Source areas for scalars and scalar fluxes, Bound.-Lay. Meteorol., 67, 293–318, 1994.
Sierra, C. A., Harmon, M. E., Moreno, F. H., Orrego, S. A., VALLE, D., and JORGE, I.: Spatial and temporal variability of net ecosystem production in a tropical forest: testing the hypothesis of a significant carbon sink, Glob. Change Biol., 13, 838–853, 2007.
Singh, K., Jardak, M., Sandu, A., Bowman, K., Lee, M., and Jones, D.: Construction of non-diagonal background error covariance matrices for global chemical data assimilation, Geosci. Model Dev., 4, 299–316, doi:10.5194/gmd-4-299-2011, 2011.
Sitch, S., McGuire, A. D., Kimball, J., Gedney, N., Gamon, J., Engstrom, R., Wolf, A., Zhuang, Q., Clein, J., and McDonald, K. C.: Assessing the carbon balance of circumpolar Arctic tundra using remote sensing and process modeling, Ecol. Appl., 17, 213–234, 2007.
Sitch, S., Huntingford, C., Gedney, N., Levy, P., Lomas, M., Piao, S., Betts, R., Ciais, P., Cox, P., and Friedlingstein, P.: Evaluation of the terrestrial carbon cycle, future plant geography and climate-carbon cycle feedbacks using five Dynamic Global Vegetation Models (DGVMs), Glob. Change Biol., 14, 2015–2039, 2008.
Sitch, S., Friedlingstein, P., Gruber, N., Jones, S. D., Murray-Tortarolo, G., Ahlström, A., Doney, S. C., Graven, H., Heinze, C., Huntingford, C., Levis, S., Levy, P. E., Lomas, M., Poulter, B., Viovy, N., Zaehle, S., Zeng, N., Arneth, A., Bonan, G., Bopp, L., Canadell, J. G., Chevallier, F., Ciais, P., Ellis, R., Gloor, M., Peylin, P., Piao, S., Le Quéré, C., Smith, B., Zhu, Z., and Myneni, R.: Trends and drivers of regional sources and sinks of carbon dioxide over the past two decades, Biogeosciences Discuss., 10, 20113–20177, doi:10.5194/bgd-10-20113-2013, 2013.
Stephens, B. B., Gurney, K. R., Tans, P. P., Sweeney, C., Peters, W., Bruhwiler, L., Ciais, P., Ramonet, M., Bousquet, P., and Nakazawa, T.: Weak northern and strong tropical land carbon uptake from vertical profiles of atmospheric CO_2, Science, 316, 1732–1735, 2007.
Suntharalingam, P., Jacob, D., Palmer, P. I., Logan, J. A., Yantosca, R. M., Xiao, Y., Evans, M. J., Streets, D. G., Vay, S. L., and Sachse, G. W.: Improved quantification of Chinese carbon fluxes using CO_2/CO correlations in Asian outflow, J. Geophys. Res.-Atmos., 109, D18S18, doi:10.1029/2003JD004362, 2004.
Susskind, J., Blaisdell, J. M., Iredell, L., and Keita, F.: Improved temperature sounding and quality control methodology using AIRS/AMSU data: the AIRS Science Team Version 5 retrieval algorithm, IEEE T. Geosci. Remote, 49, 883–907, 2011.

ACPD
14, 22587–22638, 2014

Takahashi, T., Sutherland, S. C., Wanninkhof, R., Sweeney, C., Feely, R. A., Chipman, D. W., Hales, B., Friederich, G., Chavez, F., and Sabine, C.: Climatological mean and decadal change in surface ocean pCO_2, and net sea–air CO_2 flux over the global oceans, Deep-Sea Res. Pt. II, 56, 554–577, 2009.

Tans, P. P., Conway, T. J., and Nakazawa, T.: Latitudinal distribution of the sources and sinks of atmospheric carbon dioxide derived from surface observations and an atmospheric transport model, J. Geophys. Res.-Atmos., 94, 5151–5172, 1989.

Tiwari, Y. K., Gloor, M., Engelen, R. J., Chevallier, F., Rödenbeck, C., Körner, S., Peylin, P., Braswell, B. H., and Heimann, M.: Comparing CO_2 retrieved from Atmospheric Infrared Sounder with model predictions: implications for constraining surface fluxes and lower-to-upper troposphere transport, J. Geophys. Res.-Atmos. 111, D17106, doi:10.1029/2005JD006681, 2006.

van der Werf, G. R., Randerson, J. T., Giglio, L., Collatz, G. J., Kasibhatla, P. S., and Arellano Jr., A. F.: Interannual variability in global biomass burning emissions from 1997 to 2004, Atmos. Chem. Phys., 6, 3423–3441, doi:10.5194/acp-6-3423-2006, 2006.

Wanninkhof, R., Park, G. -H., Takahashi, T., Sweeney, C., Feely, R., Nojiri, Y., Gruber, N., Doney, S. C., McKinley, G. A., Lenton, A., Le Quéré, C., Heinze, C., Schwinger, J., Graven, H., and Khatiwala, S.: Global ocean carbon uptake: magnitude, variability and trends, Biogeosciences, 10, 1983–2000, doi:10.5194/bg-10-1983-2013, 2013.

Wecht, K. J., Jacob, D. J., Wofsy, S. C., Kort, E. A., Worden, J. R., Kulawik, S. S., Henze, D. K., Kopacz, M., and Payne, V. H.: Validation of TES methane with HIPPO aircraft observations: implications for inverse modeling of methane sources, Atmos. Chem. Phys., 12, 1823–1832, doi:10.5194/acp-12-1823-2012, 2012.

Williams, M., Richardson, A. D., Reichstein, M., Stoy, P. C., Peylin, P., Verbeeck, H., Carvalhais, N., Jung, M., Hollinger, D. Y., Kattge, J., Leuning, R., Luo, Y., Tomelleri, E., Trudinger, C. M., and Wang, Y.-P.: Improving land surface models with FLUXNET data, Biogeosciences, 6, 1341–1359, doi:10.5194/bg-6-1341-2009, 2009.

Xiong, X., Barnet, C., Wei, J., and Maddy, E.: Information-based mid-upper tropospheric methane derived from Atmospheric Infrared Sounder (AIRS) and its validation, Atmos. Chem. Phys. Discuss., 9, 16331–16360, doi:10.5194/acpd-9-16331-2009, 2009.

Yevich, R. and Logan, J. A.: An assessment of biofuel use and burning of agricultural waste in the developing world, Global Biogeochem. Cy., 17, 1095, doi:10.1029/2002GB001952, 2003.

ACPD
14, 22587–22638, 2014

Yu, G. R., Zhu, X. J., Fu, Y. L., He, H. L., Wang, Q. F., Wen, X. F., Li, X. R., Zhang, L. M., Zhang, L., and Su, W.: Spatial patterns and climate drivers of carbon fluxes in terrestrial ecosystems of China, Glob. Change Biol., 19, 798–810, 2013.

Zhang, L., Jacob, D. J., Kopacz, M., Henze, D. K., Singh, K., and Jaffe, D. A.: Intercontinental source attribution of ozone pollution at western US sites using an adjoint method, Geophys. Res. Lett., 36, L11810, doi:10.1029/2009GL037950, 2009.

Zhu, Q. and Zhuang, Q.: Improving the quantification of terrestrial ecosystem carbon dynamics over the United States using an adjoint method, Ecosphere, 4, 118, L11810, doi:10.1890/ES13-00058.1, 2013a.

Zhu, Q. and Zhuang, Q.: Influences of calibration data length and data period on model parameterization and quantification of terrestrial ecosystem carbon dynamics, Geosci. Model Dev. Discuss., 6, 6835–6865, doi:10.5194/gmdd-6-6835-2013, 2013b.

Zhu, Q. and Zhuang, Q.: Modeling the effects of organic nitrogen uptake by plants on the carbon cycling of boreal forest and tundra ecosystems, Biogeosciences, 10, 7943–7955, doi:10.5194/bg-10-7943-2013, 2013c.

Zhu, Q. and Zhuang, Q.: Parameterization and sensitivity analysis of a process-based terrestrial ecosystem model using adjoint method, J. Adv. Model. Earth Sys., 6, 315–331, 2014.

Zhuang, Q., McGuire, A., Melillo, J., Clein, J., Dargaville, R., Kicklighter, D., Myneni, R., Dong, J., Romanovsky, V., and Harden, J.: Carbon cycling in extratropical terrestrial ecosystems of the Northern Hemisphere during the 20 century: a modeling analysis of the influences of soil thermal dynamics, Tellus B, 55, 751–776, 2003.

Zhuang, Q., He, J., Lu, Y., Ji, L., Xiao, J., and Luo, T.: Carbon dynamics of terrestrial ecosystems on the Tibetan Plateau during the 20th century: an analysis with a process-based biogeochemical model, Global Ecol. Biogeogr., 19, 649–662, 2010.

ACPD
14, 22587–22638, 2014

Table 1. Parameters involved in TEM calibration.

ID	Definition	Unit	Empirical range	Related processes
C_{MAX}	Maximum rate of photosynthesis C	$g\,C\,m^{-2}\,mon^{-1}$	[50, 1500]	Photosynthesis
K_I	Half saturation constant for PAR used by plants	$J\,cm^{-2}\,day^{-1}$	[20, 600]	Photosynthesis
K_C	Half saturation constant for CO_2-C uptake by plants	$\mu L\,L^{-1}$	[20, 600]	Photosynthesis
A_{LEAF}	Coefficient A of leaf phenology to model the relative photosynthetic capacity of vegetation	None	[0.1, 1.0]	Photosynthesis
B_{LEAF}	Coefficient B of leaf phenology to model the relative photosynthetic capacity of vegetation	None	[0.1, 1.0]	Photosynthesis
C_{FALL}	Proportion of vegetation carbon loss as litter-fall monthly	$g\,g^{-1}\,mon^{-1}$	[0.001, 0.015]	Photosynthesis
RA_{Q10A0}	Leading coefficient of the Q10 model for plant respiration	None	[1.3502, 3.3633]	Plant respiration
K_R	Plant respiration rate at 0 °C	$g\,g^{-1}\,mon^{-1}$	[3.1610^{-8}, 0.0316]	Plant respiration
RH_{Q10}	Change in heterotrophic respiration rate due to 10 °C temperature change	None	[1.0, 3.0]	Soil respiration
K_{DC}	Heterotrophic respiration rate at 0 °C	$g\,g^{-1}\,mon^{-1}$	[0.0005, 0.007]	Soil respiration
N_{MAX}	Maximum rate of N uptake by vegetation	$mg\,N\,m^{-2}\,mon^{-1}$	[500, 700]	N dynamics
K_{N1}	Half saturation constant for N uptake by vegetation	$mg\,cm^{-3}$	[0.0005, 0.010]	N dynamics
N_{UP}	Ratio between N immobilized and C respired by heterotrophs	$mg\,g^{-1}$	[5, 100]	N dynamics
K_{N2}	Half saturation constant for net mineralization	$mg\,cm^{-3}$	[0.0005, 0.010]	N dynamics
N_{FALL}	Proportion of vegetation nitrogen loss as litter-fall monthly	$g\,g^{-1}\,mon^{-1}$	[0.003, 0.012]	N dynamics

ACPD
14, 22587–22638, 2014

Table 2. AmeriFlux sites used for TEM model calibration and validation.

	Plant functional type	longitude, latitude	Available data	References
Calibration sites				
Atqasuk	Tundra	157.41° W, 70.46° N	2003–2005	Falge et al. (2002)
UCI 1989	Boreal forest	98.96° W, 55.91° N	2001–2002, 2004–2005	Goulden et al. (2006)
Blodgett Forest	Temperate coniferous	120.63° W, 38.89° N	1999–2006	Misson et al. (2006)
Harvard Forest	Temperate deciduous	72.17° W, 42.53° N	1992–2006	Urbanski et al. (2007)
Vaira Ranch	Grass	120.95° W, 38.40° N	2001–2007	Baldocchi et al. (2004)
Sky Oaks New	Shrub	116.64° W, 33.38° N	2004–2006	H. Luo et al. (2007)
LBA Tapajos KM83 Logged Forest	Tropical forest	54.971° W, 3.01° N	2000–2003	Miller et al. (2004)
Freeman Ranch Mesquite Juniper	Xeric woodland	97.996° W, 29.94° N	2004–2006	Litvak et al. (2010)
Validation sites				
Barrow	Tundra	156.63° W, 71.32° N	1999, 2001	Eugster et al. (2000)
UCI 1850	Boreal forest	98.48° W, 55.87° N	2003–2005	Goulden et al. (2006)
Niwot Ridge	Temperate coniferous	105.55° W, 40.03° N	1998–2007	Turnipseed et al. (2003)
Bartlett Experimental Forest	Temperate deciduous	71.28° W, 44.06° N	2004–2006	Ollinger and Smith (2005)
Fort Peck	Grass	105.10° W, 48.30° N	2000–2006	Gilmanov et al. (2005)
Lost Creek	Shrub	89.97° W, 46.08° N	2001–2005	Sulman et al. (2009)
LBA Tapajos KM67 Mature Forest	Tropical forest	54.95° W, 2.85° N	2003–2004	Grant et al. (2009)
Tonzi Ranch	Xeric woodland	120.97° W, 38.43° N	2001–2007	Ma et al. (2011)

ACPD
14, 22587–22638, 2014

Table 3. Global-view CO_2 inland sites reserved for model validation.

ID	Lon	Lat	Elevation (m)	Continent	Site	Observation type
1	−40.53	144.3	500	Australia	Bass Strait/Cape Grim, Tasmania, Australia	Aircraft
2	−8.92	−56.79	250	South America	Alta Floresta, Brazil	Aircraft
3	23.2625	5.6322	2715	Africa	Assekrem, Algeria	Surface flask
4	44.1776	28.6647	5	Europe	Black Sea, Constanta, Romania	Surface flask
5	36.607	−97.489	374	North America	Southern Great Plains, Oklahoma, US	Surface in situ
6	44.4516	111.0956	1012	Asia	Ulaan Uul, Mongolia	Surface flask

ACPD
14, 22587–22638, 2014

Table 4. Posterior mean terrestrial carbon fluxes ($Pg\,C\,yr^{-1}$) in 2003, aggregated at 11 TransCom land regions. We compare five independent inversions from CarboScope (www.carboscope.eu) with our estimations.

	Lsce_an_v2.1	CarbonTracker _CTE2008	Jena_s96_v3.3	Lsce_var_v1.0	Jena_s99_v3.3	CarboScope mean and std	GC-TEM (this work)	GC-CASA (this work)
N America boreal	−0.28	−0.27	0.08	0.15	−0.11	−0.086 ± 0.197	−0.1847	0.0759
N America temperate	0.06	−0.54	−0.44	−0.27	−0.7	−0.378 ± 0.290	−0.9305	−1.0099
S America tropic	−0.15	0.13	−0.08	0.44	−0.23	0.022 ± 0.269	−0.2438	0.6226
S America temperate	0.03	−0.04	−0.08	0.38	−0.07	0.044 ± 0.192	0.0056	−0.6528
N Africa	0.21	0.09	0.23	−0.32	−0.29	−0.016 ± 0.269	0.0245	−0.2661
S Africa	0.58	0.26	−0.06	0.16	−0.14	0.16 ± 0.284	−0.1164	−1.0378
Eurasia boreal	−0.34	−0.48	−0.41	−0.09	−0.62	−0.388 ± 0.196	−0.1244	−0.474
Eurasia temperate	−0.45	−0.25	−1.42	−0.55	−0.45	−0.624 ± 0.458	−0.3673	−0.6508
Asia tropic	−0.5	0.01	−0.22	−0.56	−0.17	−0.288 ± 0.237	−0.0303	−0.1538
Australia	0.14	0.06	0	0.02	0	0.044 ± 0.058	−0.1468	−0.1859
Europe	−0.08	−0.08	−0.35	−0.52	−0.39	−0.284 ± 0.196	−0.3637	−0.7267

ACPD
14, 22587–22638, 2014

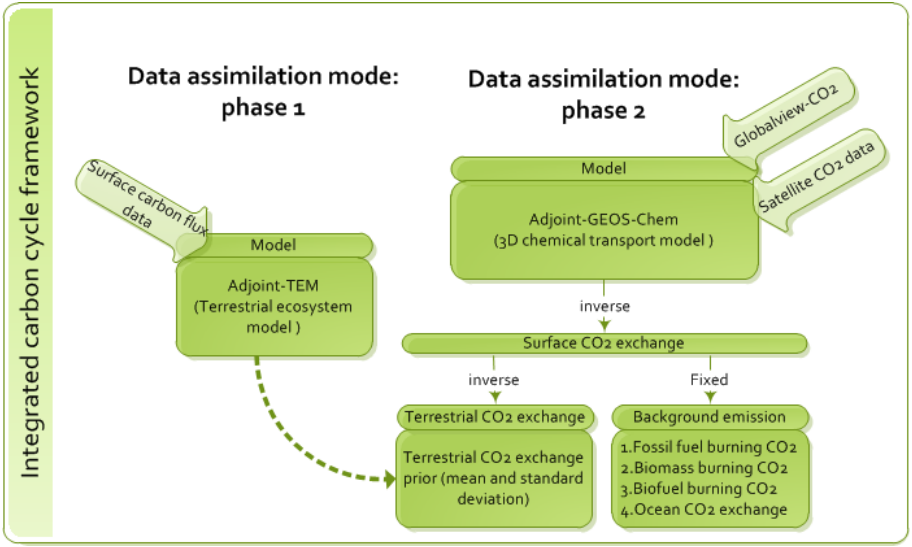

Figure 1. Modeling framework.

ACPD
14, 22587–22638, 2014

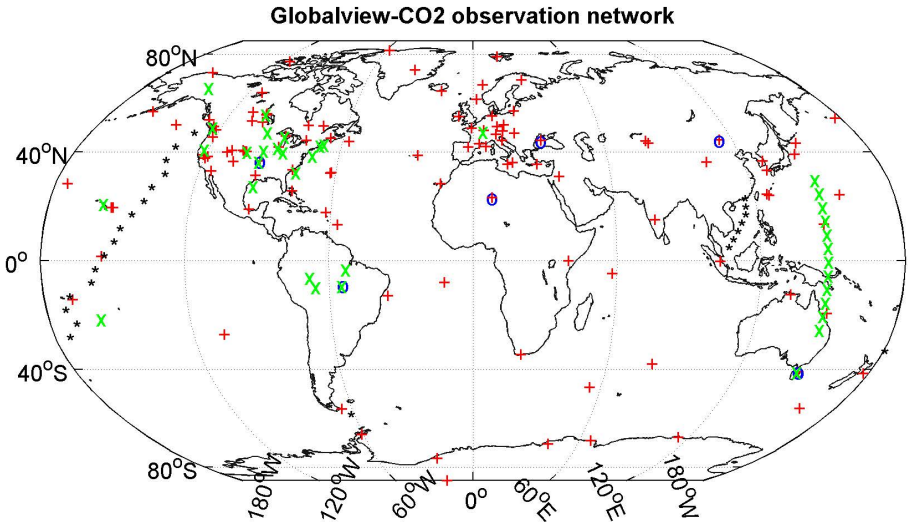

Figure 2. Globalview-CO_2 surface observational network, including surface stationary sites (red '+'), airplane (green 'x') and ship (black '*') sampling. Six sites are reserved for model validation (blue 'o').

ACPD
14, 22587–22638, 2014

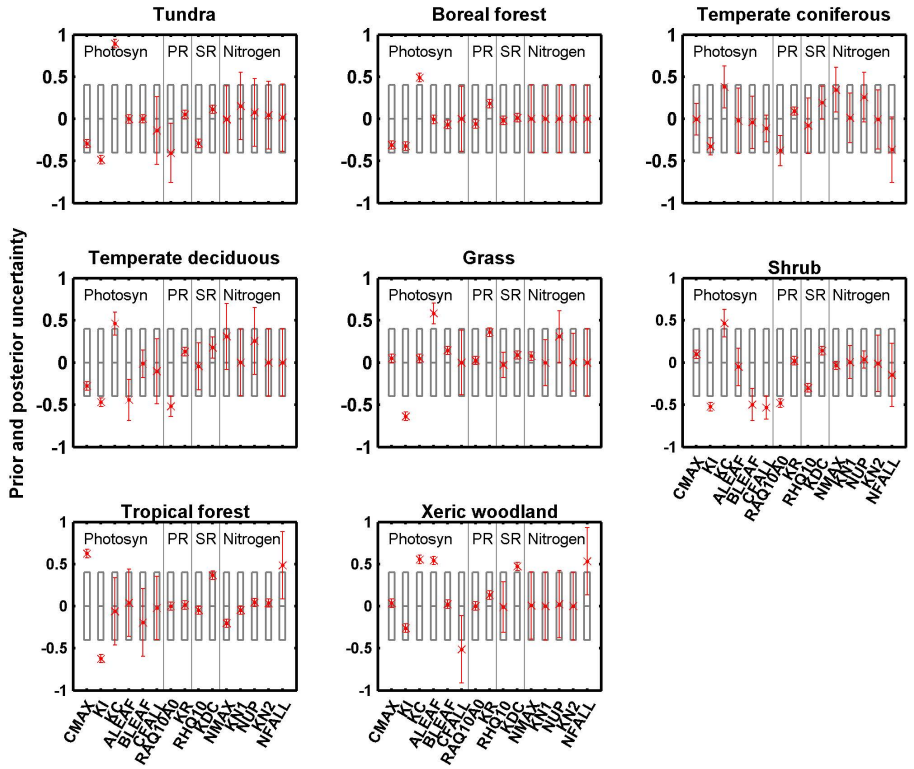

Figure 3. Prior and posterior model parameters and associated uncertainties. Grey boxes are normalized prior parameter values and uncertainties. Red star and error bars are normalized posterior parameter values and uncertainties. The 15 parameters are grouped into four categories: (1) photosynthesis (Photosyn); (2) plant respiration (PR); (3) soil respiration (SR); and (4) nitrogen processes (Nitrogen).

ACPD
14, 22587–22638, 2014

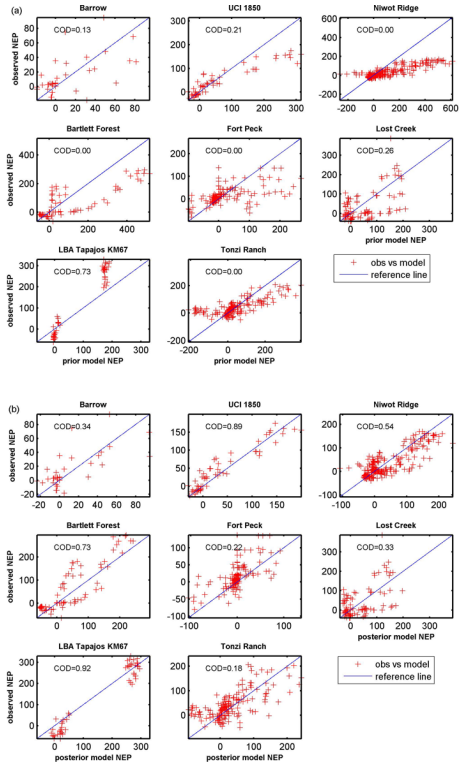

Figure 4. (a) Prior model and **(b)** Posterior model are validated against AmeriFlux observations: x-axis is simulated NEP and y-axis is AmeriFlux observed NEP. Coefficient of determination (COD: Eq. 13) is used to evaluate the model-data misfit.

ACPD
14, 22587–22638, 2014

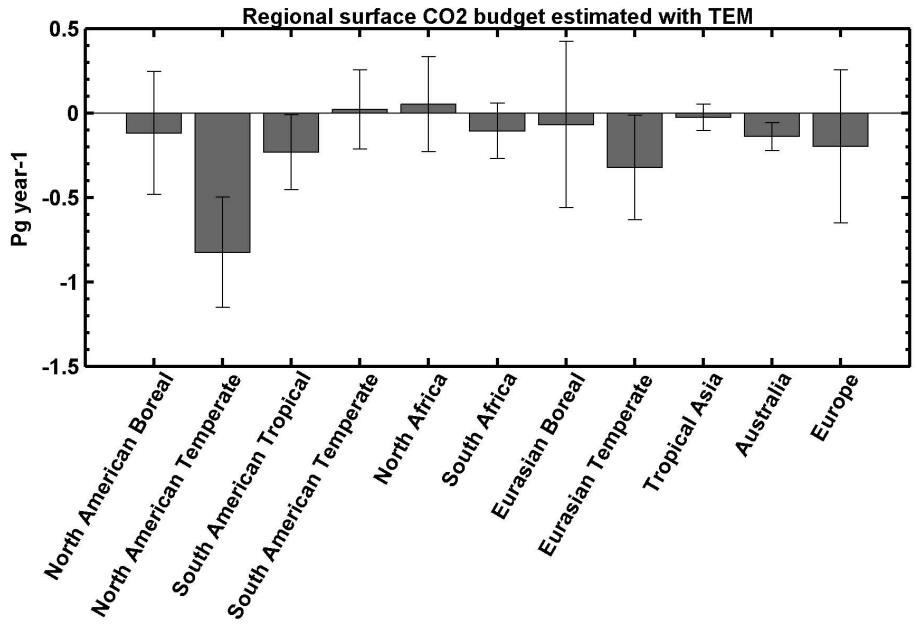

Figure 5. Net ecosystem carbon flux estimated with bottom-up approach for eleven sub-continental regions. Negative values indicate carbon sinks and positive values indicate carbon sources to the atmosphere.

ACPD
14, 22587–22638, 2014

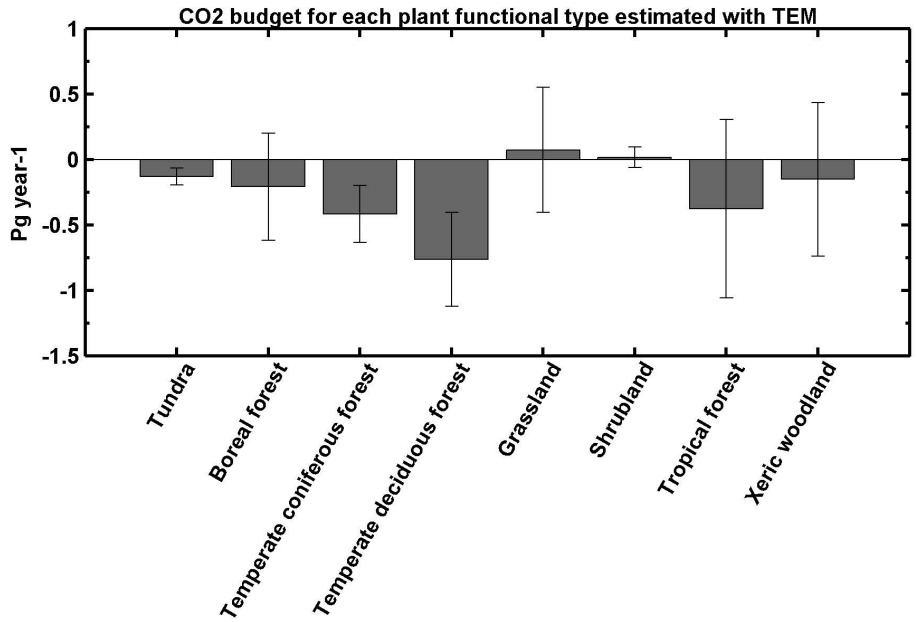

Figure 6. Net ecosystem carbon flux estimated with bottom-up approach for 8 basic plant functional types. Negative values indicate carbon sinks and positive values indicate carbon sources to the atmosphere.

ACPD
14, 22587–22638, 2014

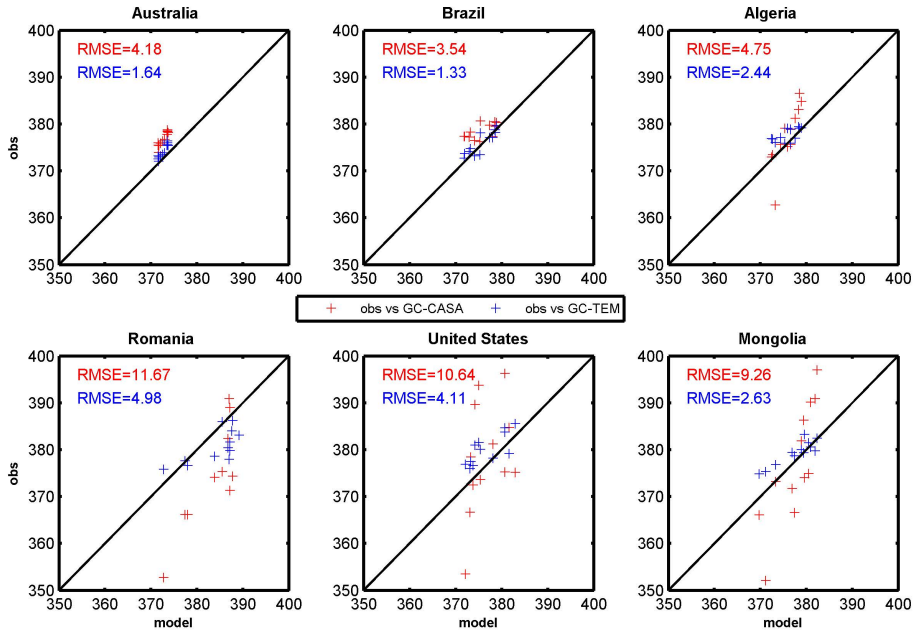

Figure 7. Posterior monthly CO_2 concentrations in 2003 from GC-TEM (blue) and GC-CASA (red) inversions, evaluated with Globalview-CO_2 representative inland sites from different continents.

ACPD
14, 22587–22638, 2014

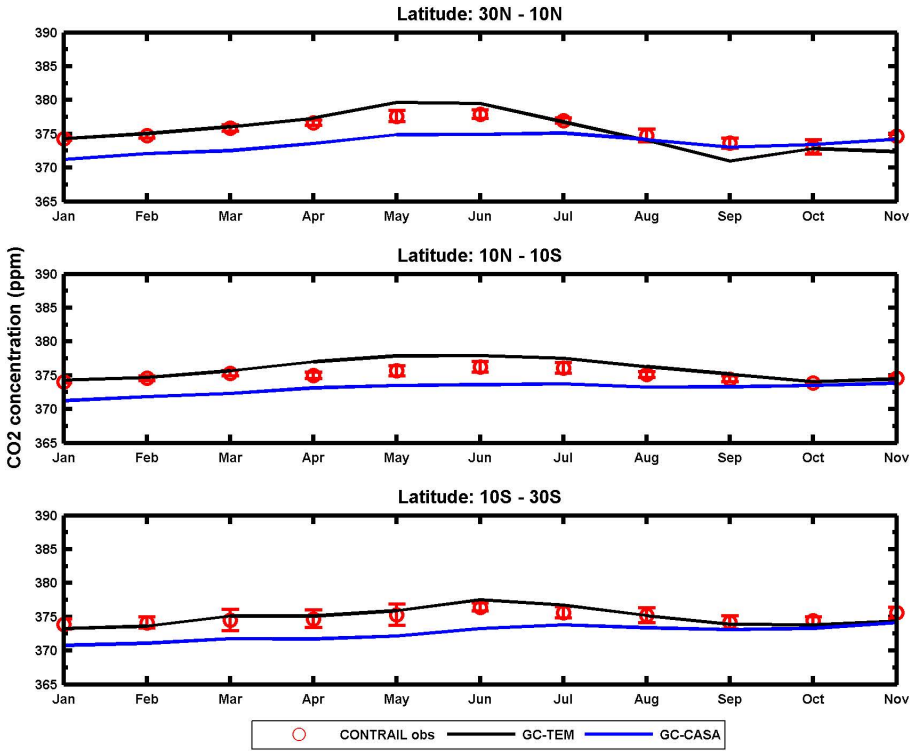

Figure 8. Posterior CO_2 concentrations in 2003 from GC-TEM (black) and GC-CASA (blue) inversions, evaluated with CONTRAIL ASE (Automatic Air Sampling Equipment) CO_2 concentration data. The CO_2 concentrations are averaged for three latitudinal bands based on CONTRAIL ASE sampling locations between 140.15° E and 152.27° E.

ACPD
14, 22587–22638, 2014